inherited. Low-expressor mutations of the AChR ε subunit are partly compensated for by expression of the embryonic AChR γ subunit, whereas the other AChR subunits have no substituting subunits. Accordingly, null and frameshift mutations are frequently detected in *CHRNE*, but not in the other subunit genes.

More than 500 patients with CMS have been reported in Western and Middle Eastern countries, whereas only four Japanese CMS patients carrying five mutations in *COLQ* encoding collagen Q that anchors acetylcholinesterase (AChE) at the NMJ have been reported by us [7,8]. Among the more than 450 CMS mutations in 19 disease genes registered in the Human Gene Mutation Database (http://www.hgmd.org), two likely have founder effects: p.Asn88Lys in *RAPSN* [9–11] and c.1124_1127dupTGCC in *DOK7* [12], whereas the others are private mutations occurring in a single or a small number of unrelated families. We here report five Japanese CMS patients with six mutations in the AChR subunit genes. We show that all the ten mutations in *COLQ*, *CHRND*, and *CHRNE* in Japanese patients are ethnically unique, which indicates that most CMS mutations arose *de novo* in recent human history or in each family.

2. Materials and methods

2.1. Ethical approval

All the human studies were approved by the institutional review boards of Nagoya University Graduate School of Medicine, Mayo Clinic, Segawa Neurological Clinic for Children, Nagoya City University, and Tokyo Women's Medical University. Appropriate written informed consent was obtained from all the patients and family members.

2.2. Mutation analysis and splicing analysis

Genomic DNA was isolated from peripheral blood with QIAamp Blood Kit (QIAGEN). We directly sequenced all exons with their flanking noncoding regions of *CHRNE*, *CHRNA1*, *CHRNB1*, and *CHRND* in this order with CEQ 8000 (Beckman Coulter). To look for large-scale DNA rearrangements in patient (Pt.) 4, we performed mate-pair sequencing of the whole genome using SOLiD4 (Life Technologies). The mate-pair library was made to span ~2 kb genomic segments according to the manufacturer's protocols. A total of 14.9 Gb of reads were mapped to human genome GRCh37/hg19 with the mapping efficiency of 89% using CLC Genomics Workbench (CLC Bio). All the reads mapped to *CHRNE* were visually scrutinized using Integrative Genome Browser (Broad Institute). Total RNA was isolated from biopsied muscle that was obtained for histopathological diagnostic purposes using RNeasy mini kit (QIAGEN). cDNA was synthesized with ReverTra Ace (Toyobo) and Oligo(dT) Primer (Life Technologies).

2.3. Expression of AChR subunit genes in HEK293 cells

Human α, β, δ, and ε subunit cDNAs were cloned into the CMV-based vector pRBG4 for expression in HEK293 cells [13]. The identified mutations were engineered into wild-type AChR subunit cDNAs in pRBG4 using the QuikChange site-directed mutagenesis kit (Stratagene). Presence of each mutation and absence of unwanted artifacts were confirmed by sequencing the entire inserts. HEK293 cells were transfected with pRBG4-α, -β, -δ, -ε, and pcDNA3.1-EGFP at a ratio of 2:1:1:1:1 using FuGENE 6 transfection reagent (Promega). After 48 hrs, cells were incubated with α-bungarotoxin Alexa Flour 647 (Life Technologies) (1:200) in PBS for 1 hr. Signals were observed under an Olympus BX60 fluorescence microscope. The cells were trypsinized, washed with PBS, and resuspended in PBS. The total number of α-bungarotoxin-binding sites on the cell surface and EGFP was determined by the FACSCalibur system (BD Biosciences).

2.4. Single channel recordings

HEK293 cells were transfected with pRBG4-α, -β, -δ, and -ε, and pEGFP-N1 at a ratio of 2:1:1:1:1, using FuGENE 6. Recordings were obtained at 24 hrs after transfection in the cell-attached configuration at a membrane potential of –80 mV at 22 °C and with bath and pipette solutions containing (in mM): KCl, 142; NaCl, 5.4; CaCl2, 1.8; MgCl2, 1.7; HEPES, 10, pH 7.4. Single-channel currents were recorded using an Axopatch 200B amplifier (Axon Instruments) at a bandwidth of 50 kHz, digitized at 5-μs intervals using Digidata 1322A (Axon Instruments) and recorded to a hard disk using the program Clampex 8.2 (Axon Instruments). Recordings obtained with ACh at 1 μM or less were analyzed at a uniform bandwidth of 10–11.7 kHz with dead time of 15.3–17.9 μs imposed. Recordings obtained with ACh at 10 μM or more were analyzed with dead time at 25 μs at 10 kHz with TAC software (Ver. x4.0.9, Bruxton). Dwell-time histograms were plotted on a logarithmic abscissa and fitted by the sum of exponentials by maximum likelihood, as previously reported [14].

3. Results

3.1. Clinical features

All Pts. had an abnormal decremental response to repetitive nerve stimulation, and no anti-AChR and anti-MuSK antibodies. Clinical features and repetitive nerve stimulation results are summarized in Table 1.

Pt. 1 (13 y.o., male) had eyelid ptosis since age six months and a positive edrophonium test. Clinical features were previously reported in a local journal [15]. Steroid pulse therapy at ages four and five years and thymectomy at age six years had no effect. Combined use of distigmine 3 mg/day and pyridostigmine 180 mg/day enabled him to sit in a chair without assistance at age 13 years. Biopsy of deltoid muscle at age eleven years showed marked AChR deficiency by fluorescent staining with α-bungarotoxin and simplified endplates by electron microscopy.

Pt. 2 (26 y.o., female) had nasal obstruction since birth and eyelid ptosis since age one month. She had a positive edrophonium test and was thought to have myasthenia gravis. Cholinesterase inhibitors were mildly effective. She has ophthamoparesis, and is able to walk but is unable to run.

Table 1
Clinical features of six patients.

Pt.	Sex	Age	Onset	Consanguinity	Repetitive N. stimulation[a]	Drug[b]
1	M	13 y	6 m	–	Accessory N., 60%; Ulnar N., 53%	Distigmine 3 mg + pyridostigmine 180 mg, effective; 3,4-DAP 40 mg, mildly effective
2	F	26 y	1 m	+	Ulnar N., 80%	Pyridostigmine 150–180 mg, mildly effective
3	F	38 y	1 y	–	Ulnar N., 81%	Pyridostigmine 90–160 mg, moderately effective
4	F	6 y	2 y	–	Median N., 60%; Ulnar N., 68%	Pyridostigmine 90 mg + 3,4-DAP 30 mg, mildly effective; ephedrine 25 mg, effective
5	M	26 y	1 m	+	Ulnar N., 76%	Pyridostigmine 135 mg, moderately effective
6	M	11 y	Birth	–	Median N., 35%; Ulnar N., 31%	Prednisolone 35 mg *dieb. alt.*, effective

[a] Repetitive N. stimulation, repetitive nerve stimulation at 2–3 Hz. Relative amplitudes of the 5th CMAP are indicated. [b] Simultaneous prescription is indicated by "+".

Pt. 3 (38 y.o., female) had ptosis at age one year and was diagnosed to have myasthenia gravis at age seven years. Since then, she has been taking cholinesterase inhibitors and prednisolone, which seemed to help but could not climb steps after age 19 years.

Pt. 4 (6 y.o., female) walked alone at age 18 months, but since age two years she had repeated episodes of generalized muscle weakness that lasted about a week, especially when having a common cold. She could walk alone but was positive for a Gowers' sign. Cholinesterase inhibitors were moderately effective. Neurological examination of the mother detected no abnormality. The father was asymptomatic according to the mother, but was not examined by us. Clinical features were previously reported as patient 4 in a local journal [16].

Pt. 5 (26 y.o., male) had feeding difficulty at age one month and had eyelid ptosis since age five months. He has weak facial muscles and is unable to run. At age seven years, he had generalized muscle weakness during an upper respiratory infection. The edrophonium test was positive.

Pt. 6 (11 y.o., male) had repeated respiratory distress and respiratory infection during infancy. He walked alone at age one year, but was noticed to walk slowly at age five years with frequent falling episodes. Rest for a short time improved his walking, but there was no diurnal fluctuation of the symptoms. Intravenous administration of edrophonium chloride ameliorated walking difficulty, but long-acting cholinesterase inhibitors had no effect.

3.2. Mutation analysis

We directly sequenced AChR subunit genes in Pts. 1–6, and identified six mutations in *CHRND* and *CHRNE*, as well as a polymorphism in *CHRNB1* (Table 2). In this study, approved nucleotide and amino acid positions are used instead of the legacy annotation, in which nucleotide and amino acid positions start from the initiation sites of mature peptides.

Pt. 1 was compound heterozygous for c.1372-1G>A at the 3′ end of intron 11 of *CHRND* and c.127C>T predicting p.Arg44Trp at the extracellular domain of the δ subunit (Fig. 1A). cDNA extracted from biopsied muscle revealed that a newly generated 'ag' dinucleotide that was one nucleotide downstream of the native 'ag' was used as a splice acceptor site (Fig. 1B), which predicted p.Glu458Argfs*20 in the long cytoplasmic loop of the δ subunit (Fig. 1A). Pt. 2 was homozygous for c.655_665del predicting p.Gly219Argfs*7 in the extracellular domain of the ε subunit (Fig. 1A). Pt. 3 was heterozygous for p.Tyr262Ter in the M1 transmembrane domain of the ε subunit (Fig. 1A). Pt. 4 was heterozygous for p.Thr284Pro in the M2 transmembrane domain of the ε subunit (Fig. 1A). Pt. 5 was homozygous for p.Leu304Arg in the short extracellular link between the M2 and M3 transmembrane domains of the ε subunit (Fig. 1A). Pt. 6 was heterozygous for p.Met465Thr close to the C-terminal end of the long cytoplasmic loop connecting the M3 and M4 transmembrane domains of AChR β subunit (Fig. 1A).

Table 2
Six mutations and one polymorphism identified in AChR subunit genes.

Pt.	Gene	Nucleotide change[c]	Amino-acid change[c]	Legacy annotation[d]	Phenotypic consequence
1	*CHRND*	c.1372-1G>A	δp.Glu458Argfs*20	δE437fs	AChR deficiency
	CHRND	c.127C>T	δp.Arg44Trp	δR23W	AChR deficiency
2[a]	*CHRNE*	c.655_665del	εp.Gly219Argfs*7	εG199fs	AChR deficiency
3[b]	*CHRNE*	c.786C>G	εp.Tyr262Ter	εY242X	AChR deficiency
4	*CHRNE*	c.850A>C	εp.Thr284Pro	εT264P	SCCMS
5[a]	*CHRNE*	c.911T>G	εp.Leu304Arg	εL284R	AChR deficiency
6	*CHRNB1*	c.1394T>C	εp.Met465Thr	βM442T	~50% shortening of AChR openings

[a] Patient is homozygous for the mutation.
[b] A mutation on another allele remains unidentified.
[c] Nucleotide and amino acid positions start from the translational start sites.
[d] In legacy annotation, nucleotide and amino acid positions start from the initiation sites of mature peptides, which are 69 nt. (23 amino acids), 63 nt. (21 amino acids), and 60 nt. (20 amino acids) downstream of the translational start sites of *CHRNB1*, *CHRND*, and *CHRNE*, respectively.

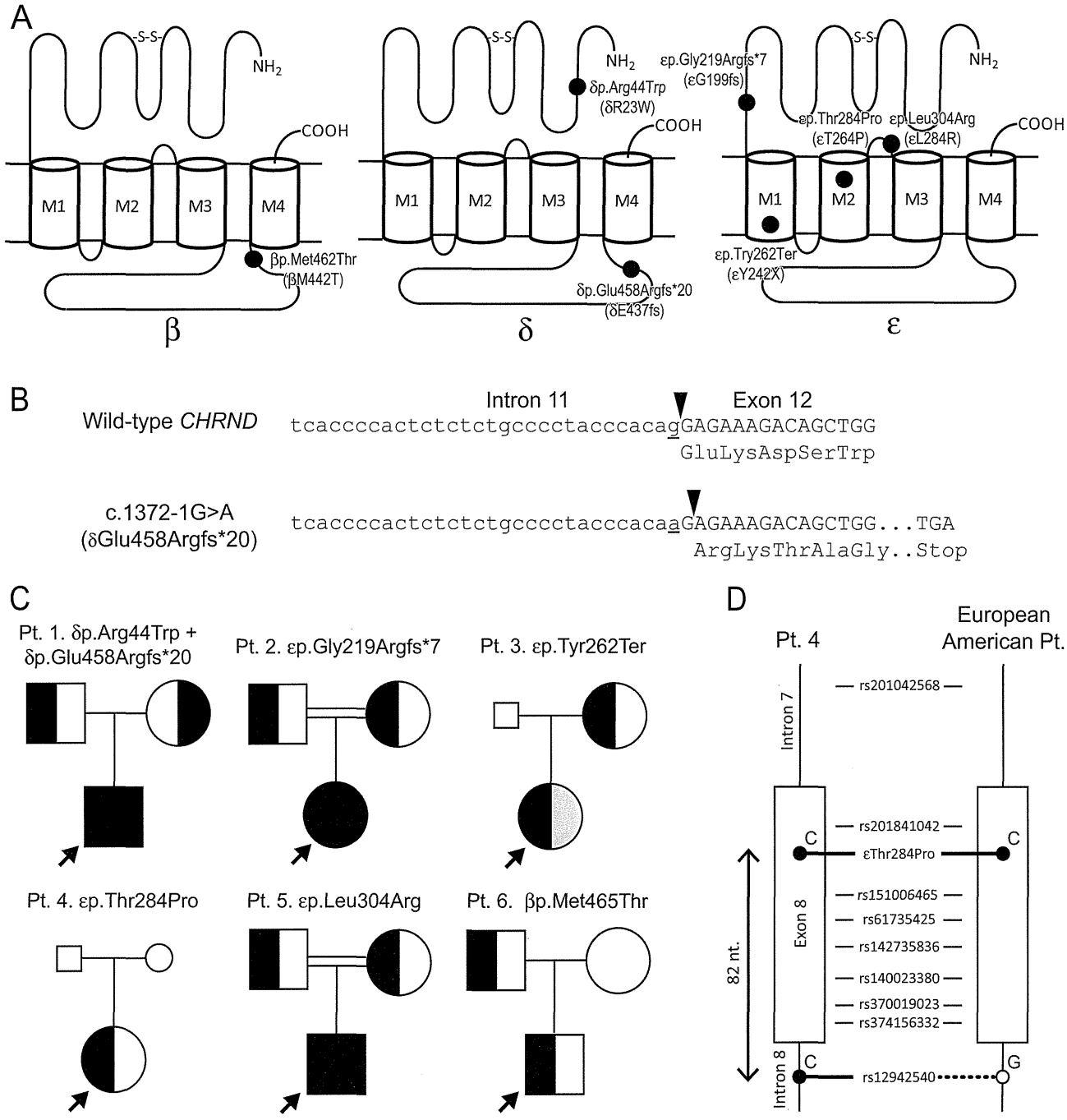

Fig. 1. Six mutations and a single polymorphism in AChR subunit genes identified in six CMS patients. (A) Positions of six mutations and a polymorphism. M1-M4, the first to fourth transmembrane domains. The M2 domains form a channel pore of AChR. (B) RT-PCR of biopsied muscle of Pt. 1 reveals that c.1372-1G>A (underlined) shifts a splice acceptor site (arrowheads) one nucleotide downstream, which predicts a shift in the reading frame (δp.Glu458Argfs*20). (C) Pedigree analyses of the mutations. Patients are indicated by arrows. Full and half shaded symbols represent homozygous and heterozygous mutations, respectively. Gray half shaded symbols represent that the individuals are predicted to carry a heterozygous mutation, the identity of which, however, has not been identified. Small symbols indicate that DNA is not available. (D) Haplotype analysis of εp.Thr284Pro in Pt. 4 and the previously reported European American Pt [7]. Both patients carry discordant nucleotides at rs12942540, which is 82 nt. downstream of the mutation.

δp.Arg44Trp (rs55868108) in Pt. 1 was previously reported in one of five healthy controls, but its ethnic origin was not documented [17]. δp.Arg44Trp, however, is not observed in the 1000 genome project (http://www.1000genomes.org/) or in the human gene variation database (HGVD), which collates SNPs in a large cohort of Japanese individuals (http://www.genome.med.kyoto-u.ac.jp/SnpDB/) [18]. As indicated below, functional analysis disclosed that δp.Arg44Trp

Table 3
Open intervals and bursts of wild-type and mutant AChR expressed on HEK cells.

	Open intervals		Bursts	
	Wild-type	βp.Met465Thr	Wild-type	βp.Met465Thr
τ_1 (ms)	0.037 ± 0.0033[a]	0.022[b]	0.036 ± 0.0017[c]	0.039 ± 0.006[d]
(a_1)	(0.17 ± 0.022)	(0.18)	(0.24 ± 0.021)	(0.18 ± 0.034)
τ_2 (ms)	0.31 ± 0.050	0.16 ± 0.017[e]	0.47 ± 0.059	0.16 ± 0.037[f]
(a_2)	(0.27 ± 0.038)	(0.23 ± 0.031)	(0.21 ± 0.027)	(0.23 ± 0.010)
τ_3 (ms)	1.35 ± 0.051	0.98 ± 0.034	3.31 ± 0.12	1.93 ± 0.085
(a_3)	(0.67 ± 0.042)	(0.78 ± 0.028)	(0.58 ± 0.038)	(0.82 ± 0.034)

Twenty-one wild-type and seven mutant patches were analyzed. Time constants, τ_n, and fractional areas, a_n, for each component are presented with mean ± SEM. ACh concentration was 50–100 nM.
[a–f] Not detected at 12, 6, 3, 5, 1, and 3 patches, respectively.
Final band widths were 11.7 and 10 kHz for wild-type and mutant AChRs, respectively.

significantly reduces cell surface expression of AChR and is unlikely to be polymorphism.

p.Met465Thr (rs201776800) in Pt. 6 was observed in eight alleles in eight Japanese individuals in the 1000 genome project with a minor allelic frequency (MAF) of 0.004, as well as in 119 alleles in a cohort of 1170 Japanese individuals in HGVD with a MAF of 0.051. Although p.Met465Thr was likely to be a polymorphism according to the high MAFs in the Japanese, we scrutinized functional consequences of p.Met465Thr in this study.

*3.3. εp.Gly219Argfs*7, εp.Tyr262Ter, and δp.Glu458Argfs*20 are predicted to compromise AChR expression*

Among the six mutations, εp.Gly219Argfs*7 in Pt. 2 and εp.Tyr262Ter in Pt. 3 were predicted to produce truncated ε subunits. We previously reported that truncation mutations in the εsubunit lead to expression of the embryonic $\alpha_2\beta\delta\gamma$-AChR at the patient's endplates and the patients have endplate AChR deficiency [19–21]. The ε mutations in Pts. 2 and 3 were thus predicted to cause AChR deficiency.

δp.Glu458Argfs*20 in Pt. 1 was predicted to generate a truncated δ subunit that cannot be incorporated into mature AChR. The phenotype of Pt. 1 is thus determined by δp.Arg44Trp on the other allele, which causes AChR deficiency as indicated below.

3.4. εp.Thr284Pro is an established slow-channel mutation without shared haplotype with a European American patient

εp.Thr284Pro in the M2 domain of the ε subunit was identical to the first characterized slow-channel mutation reported in a patient of Swiss and Turkish descent [22]. We asked if the mutation in Pt. 4 derived from the same founder allele as the first reported patient. Therefore we sequenced exon 8 and its flanking intronic regions where nine SNPs were located (Fig. 1C). This revealed that the mutant allele in the Japanese patient had 'C', whereas the mutant allele in the European American patient had 'G' at rs12942540 in intron 8, which was located 82 nt. downstream of εp.Thr284Pro. Accordingly, εp.Thr284Pro in both patients is likely to have occurred independently in two ethnic groups.

3.5. δp.Arg44Trp and εp.Leu304Arg, but not βp.Met465Thr, decrease cell surface expression of AChR in transfected HEK293 cells

We next analyzed the effects of AChR expression of the remaining three mutations of δp.Arg44Trp, εp.Leu304Arg and βp.Met465Thr. We introduced wild-type or mutant α, β, δ, and ε subunit cDNAs along with EGFP cDNA into HEK293 cells (Fig. 2A), and measured cell surface expression of AChR detected by Alexa 647-labeled α-bungarotoxin using FACS. Expression of βp.Met465Thr-AChR was similar to that of wild-type AChR, whereas δp.Arg44Trp and εp.Leu304Arg markedly attenuated the cell surface expression of AChR (Figs. 2B and C). Accordingly, δp.Arg44Trp and εp.Leu304Arg cause endplate AChR deficiency.

3.6. βp.Met465Thr mildly shortens channel opening events, but not as much as the other established fast channel mutations

As βp.Met465Thr-AChR was efficiently expressed on HEK293 cells, we next recorded opening and closing of single AChR channels at limiting low concentrations of ACh by the patch clamp method (Fig. 3A). We found that the major burst duration (τ_3) was decreased from 3.31 ms to 1.93 ms (58.3%) in βp.Met465Thr-AChR (Table 3), while the conductance of βp.Met465Thr-AChR was normal. Distributions of opening probabilities of the clusters generated by 10 μM or greater concentrations of ACh made single peaks for both wild-type and mutant AChRs. Thus, βMet465Thr mildly shortens the channel openings but does not cause a mode switching in the kinetics of the receptor activation, which is seen in other FCCMS mutations [23,24].

3.7. A recessive mutation on the other allele in Pt. 3 remains unidentified

Functional prediction and characterization of the six mutations indicated that εp.Thr284Pro in Pt. 4 was a dominant slow-channel mutation [22], whereas the other five mutations in Pts. 1, 2, 3, and 5 were recessive loss-of-function mutations. The mutations in Pts. 1, 2, and 5 were biallelic, whereas a mutation was detected only on a single allele in Pt. 3 (Fig. 1C).

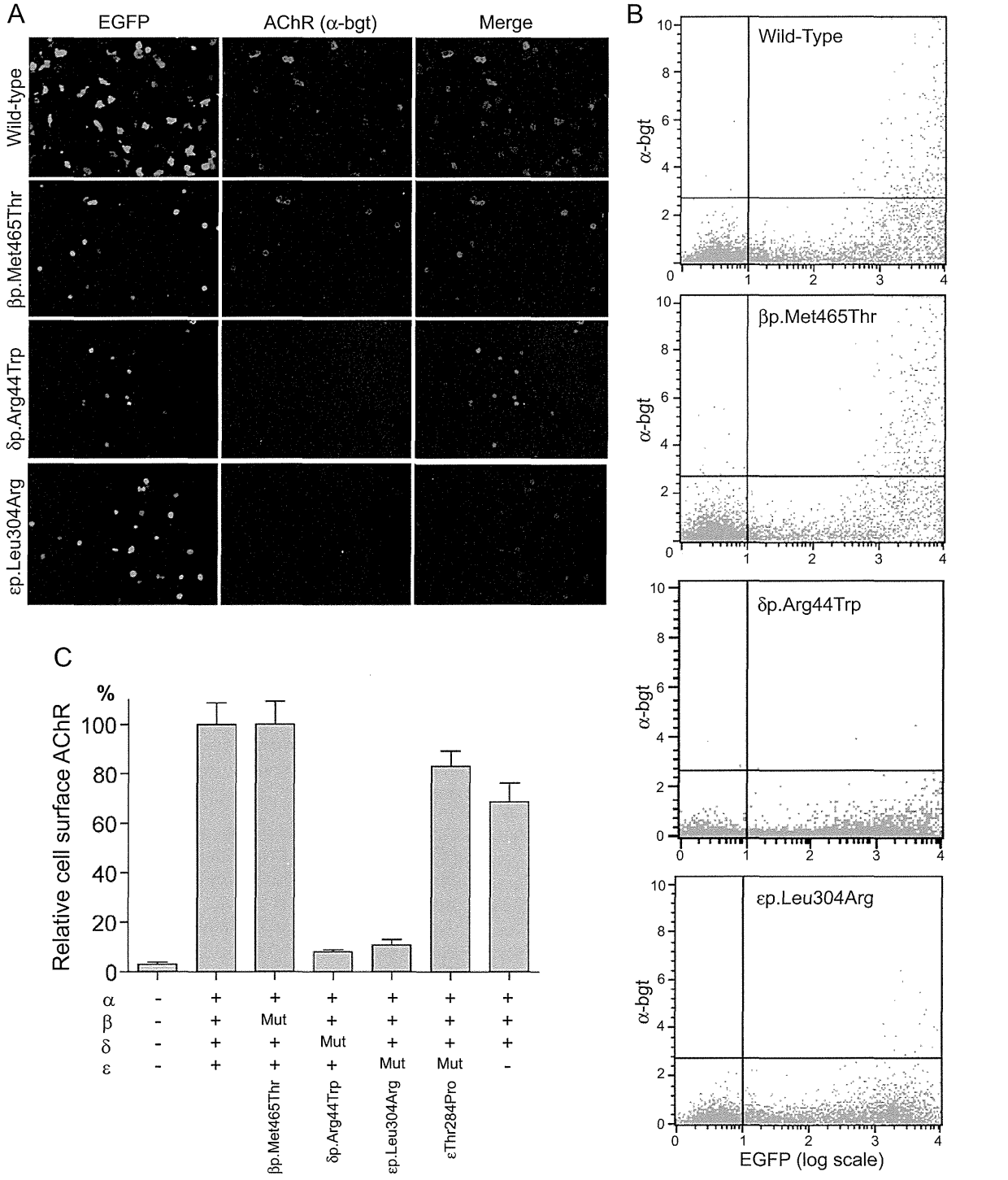

Fig. 2. Quantification of cell surface expression of wild-type and mutant AChRs on HEK293 cells. (A) HEK293 cells are transfected with wild-type or mutant AChR subunit cDNAs along with EGFP cDNA. Only transfected cells have EGFP signals and AChRs that are visualized with Alexa 647-labeled α-bungarotoxin (bgt). εp.Leu304Arg-AChR has less signals for AChRs compared to wild-type and βp.Met465Thr-AChRs. (B) Representative FACS profiles of EGFP and Alexa 647-labeled α-bgt. Both axes are shown in arbitrary units. The number of cells fractioned into the upper right quadrant is counted as AChR-positive cells. (C) Ratios of AChR-positive cells (the upper right quadrant) divided by EGFP-positive cells (the lower right quadrant). δp.Arg44Trp and εp.Leu304Arg markedly decrease AChR expression, whereas βp.Met465Thr and εp.Thr284Pro have no effect on AChR expression. ε-deficient $\alpha_2\beta\delta_2$-AChR are expressed at ~70% of wild-type, as we reported previously [21]. Mut, a mutant AChR subunit. Mean and SE are indicated ($n = 12$).

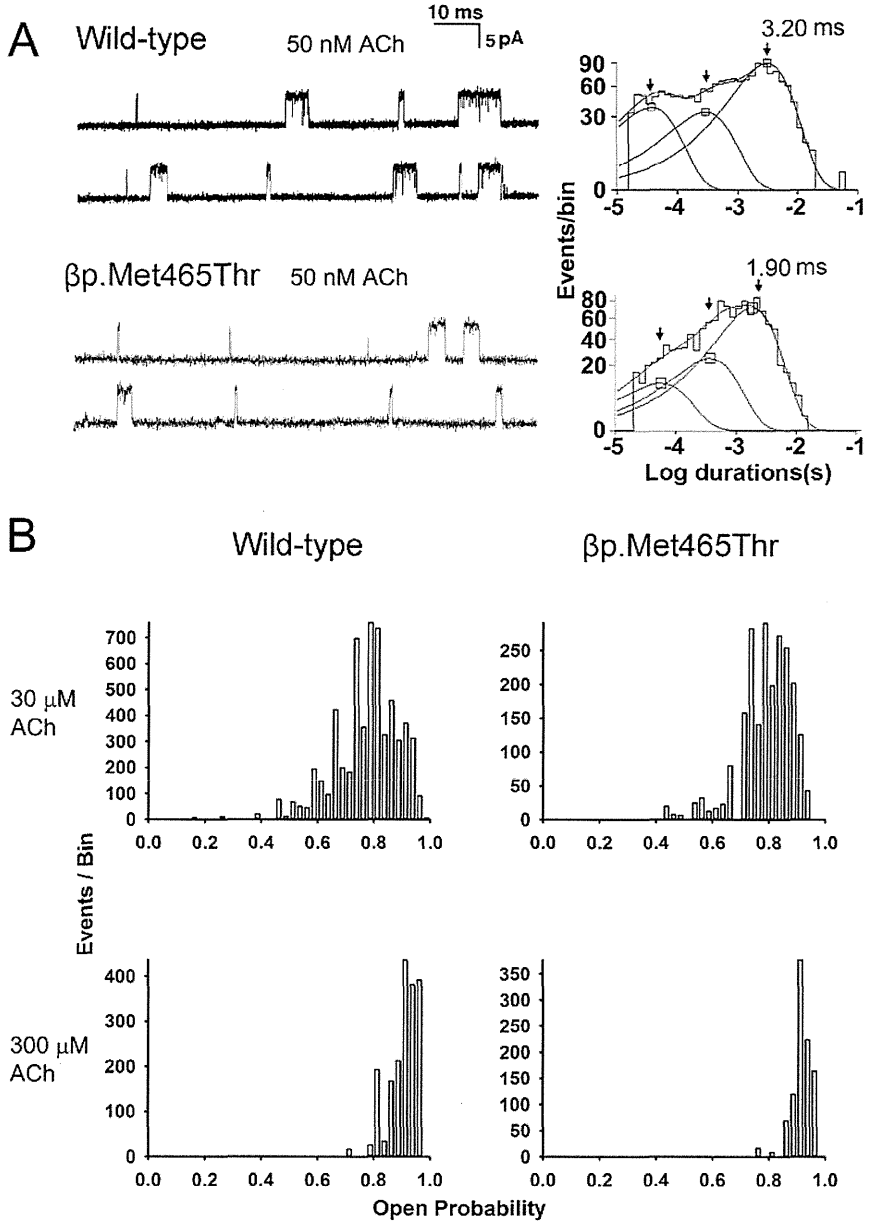

Fig. 3. Single channel currents of wild-type and mutant AChRs on HEK293 cells. (A) Left: Representative channel openings shown as upward deflections. Right: Burst duration histograms fitted to the sum of exponentials. Arrows indicate mean durations of dominant burst components. (B) Distribution of open probabilities from individual clusters obtained at the indicated ACh concentrations. Note that both wild-type and mutant AChRs make a single peak.

We scrutinized all exonic nucleotides in *CHRNE* in Pt. 3 by bidirectional sequencing, but detected none. We therefore hypothesized that a mutation on the other alleles was either a promoter mutation, a splice-site mutation disrupting a deep intronic splicing *cis*-element, or a large-scale DNA rearrangement. Sequencing of ~1 kb upstream of the translation initiation sites, however, revealed no mutation. We further analyzed genomic DNA by mate-pair sequencing of the whole genome. A total of 57 reads were mapped to *CHRNE*. Visual inspection of these reads, however, failed to detect any large-scale DNA rearrangements or any mutations. A recessive mutation on the other allele in *CHRNE* in Pt. 3 thus remains unidentified. We also analyzed 18 other CMS-causing genes using the mate-pair sequencing data in Pt. 3. As the mate-pair sequencing was for detecting a large-scale DNA rearrangement, the 18 genes were covered by only 10,116 reads. Although the coverage was not high enough for detecting SNVs, no candidate mutations were detected in Pt. 3.

Table 4
Fifteen previously reported FCCMS mutations and the currently analyzed βp.Met462Thr polymorphism.

Mutation	Burst duration (ms)			Expression	Domain	Reference
	Wild-type	Mutant	Ratio	(%)		
αp.Val152Leu (αV132L)	3.31	0.50	0.151	135	Extracellular domain of α	[25]
αp.Val208Met (αV188M)	3.31	0.68	0.205	90	Extracellular domain of α	[26]
αp.Phe276Leu (αF256L)	3.62	0.30	0.083	102	M2 domain of α	[27]
αp.Val305Ile (αV285I)	2.99	0.34	0.114	116	M3 domain of α	[28]
δp.Leu63Pro (δL42P)	3.31	0.18	0.054	37	Extracellular domain of δ	[14]
δp.Glu80Lys (δE59K)	5.06	2.75	0.543	62	Extracellular domain of δ	[29]
δp.Pro271Gln (δP250Q)	3.31	1.54	0.465	60	M1 domain of δ	[30]
εp.Thr58Lys (εT38K)	5.86	0.06	0.010	78	Extracellular domain of ε	[31]
εp.Trp75Arg (εW55R)	3.31	0.37	0.112	86	Extracellular domain of ε	[32]
εp.Pro141Leu (εP121L)	2.99	0.45	0.151	102	Extracellular domain of ε	[13]
εp.Asp195Asn (εD175N)	2.13	0.49	0.230	117[b]	Extracellular domain of ε	[33]
εp.Asn202Tyr (εN182Y)	2.13	0.65	0.305	117[b]	Extracellular domain of ε	[33]
εp.Ser433_Glu438dup (ε1254ins18)	2.80	1.01	0.361	47	Long cytoplasmic loop of ε	[23]
εp.Ala431Pro (εA411P)	n.a.[a]	n.a.[a]	n.a.[a]	31	Long cytoplasmic loop of ε	[24]
εp.Asn456del (εN436del)	3.31	1.24	0.375	51	Long cytoplasmic loop of ε	[34]
βp.Met462Thr (βM442T)	3.31	1.93	0.583	99	Long cytoplasmic loop of β	Current study

A major component of burst durations of wild-type and mutant AChRs expressed in HEK293 cells is indicated. Cell surface expression in HEK293 cells is normalized to that of wild-type. Channel openings are elicited by 50–100 nM ACh. Mutations in parentheses are legacy annotations used in original reports.

[a] Detailed ion channel kinetics are analyzed using a hidden Markov model, but burst durations are not indicated.

[b] Cell surface expression of recombinant AChR is not indicated, and the expression ratio is calculated from α-bungarotoxin binding sites of control and patient endplates.

4. Discussion

We identified six mutations in AChR subunit genes in five Japanese patients with CMS. We initially assumed that βp.Met465Thr in Pt. 6 was a mild fast-channel mutation. However, expansion of the SNP database later disclosed that βp.Met465Thr is a polymorphism that is frequently observed in the Japanese population. Fifteen previously reported FCCMS mutations shorten burst durations to 22.6 ± 16.1% of wild-type (mean and SD; range 1.0%–54.3%) (Table 4). A FCCMS mutation, δp.Glu80Lys (δE59K), decreases burst durations to 54.3% of wild-type [29], which is similar to 58.3% observed in the current βp.Met465Thr polymorphism. However, in contrast to βp.Met465Thr, δp.Glu80Lys reduces cell surface expression of AChR to 62% of wild-type [29]. Similarly, δp.Pro271Gln (δP250Q) mildly reduces burst durations to 46.5% of wild-type, but again, unlike βp.Met465Thr, this mutation reduces cell surface expression of AChR to 60% of wild-type [30]. A plot of normalized burst durations and normalized cell surface expressions suggests that a mean burst duration of less than ~30% causes FCCMS even when it does not affect the cell surface expression of AChR (Fig. 4). In contrast, a mean burst duration of between ~30% and ~60% causes FCCMS when the mutation reduces the cell surface expression of AChR to ~60% or less (Fig. 4). However, as no individual is homozygous for βp.Met465Thr or carries a null mutation on the other allele, pathogenicity of βp.Met465Thr in the absence of a normal *CHRND* on the other allele still remains unknown.

δp.Arg44Trp is close to the N-terminal end of the extracellular region (Fig. 5). We previously reported that a similar εp.Arg40Trp also causes AChR deficiency [35]. The specific function of this region, however, is not well dissected. εp.Leu304Arg is in the short extracellular link between the M2 and M3 transmembrane domains (Fig. 5). The functions of this link are not well characterized. In this link, only αp.Ser289Ile (αS269I) is reported in SCCMS [38]. βp.Met465Thr is located close to the C-terminal end of the long cytoplasmic loop that links the M3 and M4 transmembrane domains (Fig. 5). Interestingly, three FCCMS mutations in the long cytoplasmic loop are clustered close to the C-terminal end of the ε subunit [23,24,34,36,37], and similarly destabilize the channel open state. Two FCCMS mutations in this region, εp.Ser433_Glu438dup (ε1254ins18) [23] and εp.Ala431Pro (εA411P) [24], disrupt the fidelity of gating and result in unstable channel kinetics. In addition, another FCCMS

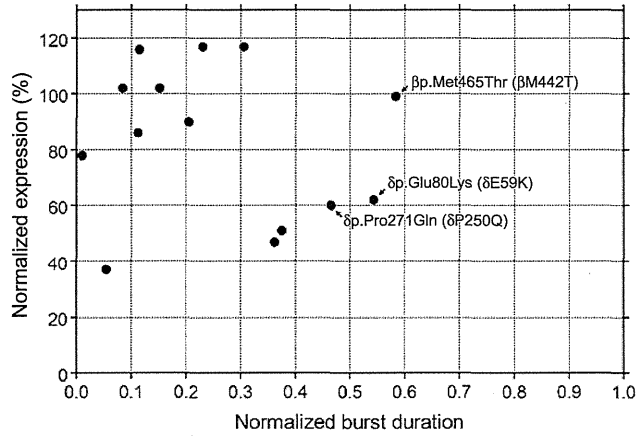

Fig. 4. Normalized burst durations and normalized cell surface expressions of previously reported FCCMS mutations and the currently analyzed βp.Met462Thr polymorphism shown in Table 4. Arrows point to mutations and a polymorphism that are addressed in the discussion.

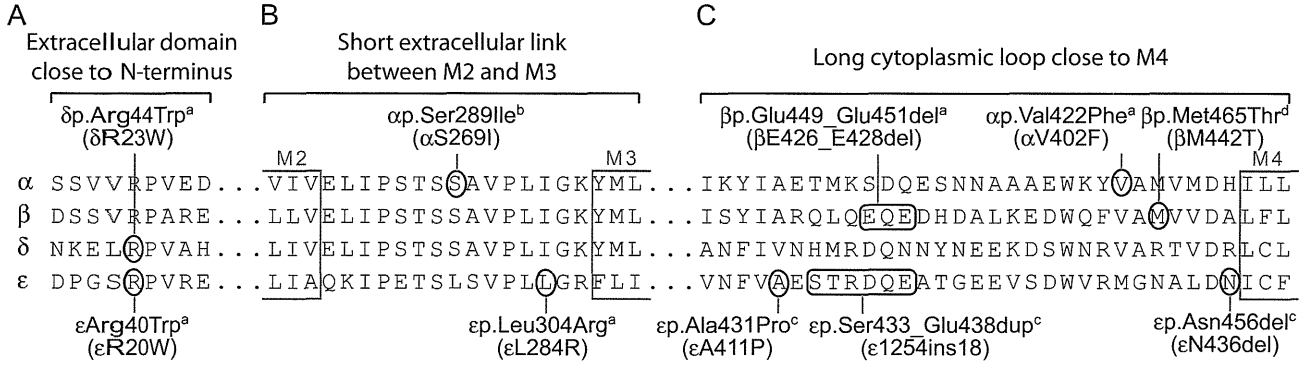

Fig. 5. Positions of the currently identified δp.Arg44Trp, εp.Leu304Arg and βp.Met465Thr, as well as previously reported CMS mutations. Mutations in the extracellular domain close the N-terminal end (A), the short extracellular link between the M2 and M3 transmembrane domains (B), and the long cytoplasmic loop close to the M4 transmembrane domain (C) are indicated. [a]δp.Arg44Trp (current report), εp.Arg40Trp [35], βp.Glu449_Glu451del [36], and αp.Val422Phe [37] cause AChR deficiency (AChR def.). [b]αp.Ser289Ile [38] causes SCCMS. [c]εp.Ala431Pro [24], ε p.Ser433_Glu438dup [23], and εp.Asn456del [34] cause FCCMS. [d]βp.Met465Thr is a currently analyzed polymorphism that shortens channel opening events. Mutations in parentheses are legacy annotations used in the original reports.

mutation in this region, εp.Asn456del (εN436del), destabilizes the diliganded receptor [34]. The C-terminal region of the long cytoplasmic loop of the ε subunit is thus likely to be crucial for stabilizing the open channel. In contrast to the three FCCMS mutations in the C-terminal end, however, βp.Met465Thr mildly shortens channel opening events and has no effect on the fidelity of channel gating, which may represent subunit-specificity and/or position-specificity of the amino acid substitutions.

Excluding δp.Arg44Trp that was previously reported in a healthy subject of unknown ethnicity [17], five of the six mutations in the AChR subunit genes in the current study and the five previously identified *COLQ* mutations [8] are unique to Japanese people. This is in contrast to some CMS mutations that are observed in unrelated families in Western and Middle Eastern countries. Especially, founder effects are implicated in two mutations: p.Asn88Lys in *RAPSN* [9–11] and c.1124_1127dupTGCC in *DOK7* [12]. CMS mutations are all recessively inherited except for those causing SCCMS. As heterozygous carriers of recessive CMS mutations exhibit no clinical phenotypes even by detailed electrophysiological studies, an asymptomatic carrier of a recessive CMS mutation has no disadvantage in transmitting the mutant allele to offspring. Lack of founder effects between the Japanese patients and patients of other nationalities thus suggest that most but not all CMS mutations arose *de novo* in a recent human history or in each family.

Acknowledgments

This study was supported by Grants-in-Aid from the MEXT and MHLW of Japan to KO. We would like to thank Dr. Andrew G. Engel for critical and constructive discussion on this project.

References

[1] Borges LS, Yechikhov S, Lee YI, et al. Identification of a motif in the acetylcholine receptor beta subunit whose phosphorylation regulates rapsyn association and postsynaptic receptor localization. J Neurosci 2008;28:11468–76.
[2] Bezakova G, Ruegg MA. New insights into the roles of agrin. Nat Rev Mol Cell Biol 2003;4:295–308.
[3] Budnik V, Salinas PC. Wnt signaling during synaptic development and plasticity. Curr Opin Neurobiol 2011;21:151–9.
[4] Korkut C, Budnik V. WNTs tune up the neuromuscular junction. Nat Rev Neurosci 2009;10:627–34.
[5] Ohno K, Ito M, Engel AG. Congenital myasthenic syndromes – molecular bases of congenital defects of proteins at the neuromuscular junction. In: Zaher A, editor. Neuromuscul. Disord. Rijeka: InTech; 2012. p. 175–200.
[6] Croxen R, Hatton C, Shelley C, et al. Recessive inheritance and variable penetrance of slow-channel congenital myasthenic syndromes. Neurology 2002;59:162–8.
[7] Ohno K, Engel AG, Brengman JM, et al. The spectrum of mutations causing endplate acetylcholinesterase deficiency. Ann Neurol 2000;47:162–70.
[8] Nakata T, Ito M, Azuma Y, et al. Mutations in the C-terminal domain of ColQ in endplate acetylcholinesterase deficiency compromise ColQ-MuSK interaction. Hum Mutat 2013;34:997–1004.
[9] Ohno K, Engel AG. Lack of founder haplotype for the rapsyn N88K mutation: N88K is an ancient founder mutation or arises from multiple founders. J Med Genet 2004;41:e8.
[10] Muller JS, Abicht A, Burke G, et al. The congenital myasthenic syndrome mutation RAPSN N88K derives from an ancient Indo-European founder. J Med Genet 2004;41:e104.
[11] Dunne V, Maselli RA. Common founder effect of rapsyn N88K studied using intragenic markers. J Hum Genet 2004;49:366–9.
[12] Ben Ammar A, Petit F, Alexandri N, et al. Phenotype genotype analysis in 15 patients presenting a congenital myasthenic syndrome due to mutations in DOK7. J Neurol 2010;257:754–66.
[13] Ohno K, Wang HL, Milone M, et al. Congenital myasthenic syndrome caused by decreased agonist binding affinity due to a mutation in the acetylcholine receptor epsilon subunit. Neuron 1996;17:157–70.
[14] Shen XM, Fukuda T, Ohno K, Sine SM, Engel AG. Congenital myasthenia-related AChR delta subunit mutation interferes with intersubunit communication essential for channel gating. J Clin Invest 2008;118:1867–76.
[15] Ishigaki K, Murakami T, Ito Y, et al. [Treatment approach to congenital myasthenic syndrome in a patient with acetylcholine receptor deficiency]. No to Hattatsu 2009;41:37–42.
[16] Irahara K, Komaki H, Honda R, et al. [Clinical features of congenital myasthenic syndrome in Japan]. No to Hattatsu 2012;44:450–4.
[17] Denning L, Anderson JA, Davis R, Gregg JP, Kuzdenyi J, Maselli RA. High throughput genetic analysis of congenital myasthenic syndromes using resequencing microarrays. PLoS ONE 2007;2:e918.

[18] Narahara M, Higasa K, Nakamura S, et al. Large-scale East-Asian eQTL mapping reveals novel candidate genes for LD mapping and the genomic landscape of transcriptional effects of sequence variants. PLoS ONE 2014;9:e100924.
[19] Engel AG, Ohno K, Bouzat C, Sine SM, Griggs RC. End-plate acetylcholine receptor deficiency due to nonsense mutations in the epsilon subunit. Ann Neurol 1996;40:810–17.
[20] Engel AG, Ohno K, Milone M, et al. New mutations in acetylcholine receptor subunit genes reveal heterogeneity in the slow-channel congenital myasthenic syndrome. Hum Mol Genet 1996;5:1217–27.
[21] Ohno K, Quiram PA, Milone M, et al. Congenital myasthenic syndromes due to heteroallelic nonsense/missense mutations in the acetylcholine receptor epsilon subunit gene: identification and functional characterization of six new mutations. Hum Mol Genet 1997;6:753–66.
[22] Ohno K, Hutchinson DO, Milone M, et al. Congenital myasthenic syndrome caused by prolonged acetylcholine receptor channel openings due to a mutation in the M2 domain of the epsilon subunit. Proc Natl Acad Sci U S A 1995;92:758–62.
[23] Milone M, Wang H-L, Ohno K, et al. Mode switching kinetics produced by a naturally occurring mutation in the cytoplasmic loop of the human acetylcholine receptor epsilon subunit. Neuron 1998;20:575–88.
[24] Wang H-L, Ohno K, Milone M, et al. Fundamental gating mechanism of nicotinic receptor channel revealed by mutation causing a congenital myasthenic syndrome. J Gen Physiol 2000;116:449–62.
[25] Shen X-M, Ohno K, Tsujino A, et al. Mutation causing severe myasthenia reveals functional asymmetry of AChR signature cystine loops in agonist binding and gating. J Clin Invest 2003;111:497–505.
[26] Shen XM, Brengman JM, Sine SM, Engel AG. Myasthenic syndrome AChRalpha C-loop mutant disrupts initiation of channel gating. J Clin Invest 2012;122:2613–21.
[27] Webster R, Brydson M, Croxen R, Newsom-Davis J, Vincent A, Beeson D. Mutation in the AChR ion channel gate underlies a fast channel congenital myasthenic syndrome. Neurology 2004;62:1090–6.
[28] Wang H-L, Milone M, Ohno K, et al. Acetylcholine receptor M3 domain: stereochemical and volume contributions to channel gating. Nat Neurosci 1999;2:226–33.
[29] Brownlow S, Webster R, Croxen R, et al. Acetylcholine receptor d subunit mutations underlie a fast-channel myasthenic syndrome and arthrogryposis multiplex congenita. J Clin Invest 2001;108:125–30.
[30] Shen XM, Ohno K, Fukudome T, et al. Congenital myasthenic syndrome caused by low-expressor fast-channel AChR delta subunit mutation. Neurology 2002;59:1881–8.
[31] Webster R, Liu WW, Chaouch A, Lochmuller H, Beeson D. Fast-channel congenital myasthenic syndrome with a novel acetylcholine receptor mutation at the alpha-epsilon subunit interface. Neuromuscul Disord 2014;24:143–7.
[32] Shen XM, Brengman JM, Edvardson S, Sine SM, Engel AG. Highly fatal fast-channel syndrome caused by AChR epsilon subunit mutation at the agonist binding site. Neurology 2012;79:449–54.
[33] Sine SM, Shen X-M, Wang H-L, et al. Naturally occurring mutations at the acetylcholine receptor binding site independently alter ACh binding and channel gating. J Gen Physiol 2002;120:483–96.
[34] Shen XM, Ohno K, Sine SM, Engel AG. Subunit-specific contribution to agonist binding and channel gating revealed by inherited mutation in muscle acetylcholine receptor M3-M4 linker. Brain 2005;128:345–55.
[35] Shen X-M, Ohno K, Milone M, Brengman JM, Spilsbury P, Engel AG Low-affinity fast-channel syndrome. Neurology 2001;56(Suppl. 3):A60. (abstract).
[36] Quiram PA, Ohno K, Milone M, et al. Mutation causing congenital myasthenia reveals acetylcholine receptor beta/delta subunit interaction essential for assembly. J Clin Invest 1999;104:1403–10.
[37] Milone M, Shen X-M, Ohno K, et al. Unusual congenital myasthenic syndrome with endplate AChR deficiency caused by alpha subunit mutations and a remitting-relapsing clinical course. Neurology 1999;51(Suppl. 2):A185. (abstract).
[38] Croxen R, Newland C, Beeson D, et al. Mutations in different functional domains of the human muscle acetylcholine receptor alpha subunit in patients with the slow-channel congenital myasthenic syndrome. Hum Mol Genet 1997;6:767–74.

Original Investigation

Impaired Synaptic Development, Maintenance, and Neuromuscular Transmission in LRP4-Related Myasthenia

Duygu Selcen, MD; Bisei Ohkawara, PhD; Xin-Ming Shen, PhD; Kathleen McEvoy, MD; Kinji Ohno, MD, PhD; Andrew G. Engel, MD

IMPORTANCE Congenital myasthenic syndromes (CMS) are heterogeneous disorders. Defining the phenotypic features, genetic basis, and pathomechanisms of a CMS is relevant to prognosis, genetic counseling, and therapy.

OBJECTIVES To characterize clinical, structural, electrophysiologic, and genetic features of a CMS and to search for optimal therapy.

DESIGN, SETTINGS, AND PARTICIPANTS Two sisters with CMS affecting the limb-girdle muscles were investigated between 2012 and 2014 at an academic medical center by clinical observation, in vitro analysis of neuromuscular transmission, cytochemical and electron microscopy studies of the neuromuscular junction, exome sequencing, expression studies in HEK293 and COS7 cells, and for response to therapy, and they were compared with 15 historical control participants.

MAIN OUTCOMES AND MEASURES We identified the disease gene and mutation, confirmed pathogenicity of the mutation by expression studies, and instituted optimal pharmacotherapy.

RESULTS Quantitative analysis of single EP regions was done for all 15 control participants and microelectrode studies of neuromuscular transmission and α-bgt binding sites per EP was conducted for 13 control participants. Examination of the older sister's intercostal muscle end plates (EPs) showed them to be abnormally small, with attenuated reactivities for the acetylcholine receptor and acetylcholinesterase. Most EPs had poorly differentiated or degenerate junctional folds, and some appeared denuded of nerve terminals. The amplitude of the EP potential (EPP), the miniature EPP, and the quantal content of the EPP were all markedly reduced. Exome sequencing identified a novel homozygous p.Glu1233Ala mutation in low-density lipoprotein receptor-related protein 4 (LRP4), a coreceptor for agrin to activate muscle-specific tyrosine kinase (MuSK), which is required for EP development and maintenance. Expression studies indicate that the mutation compromises the ability of LRP4 to bind to, phosphorylate, and activate MuSK. Treatment with albuterol sulfate improved the patients' symptoms. A previously identified patient harboring 2 heterozygous mutations in LRP4 had structurally abnormal intercostal EPs but no identifiable defect of neuromuscular transmission at these EPs.

CONCLUSIONS AND RELEVANCE We identified a second CMS kinship harboring mutations in *LRP4*, identified the mechanisms that impair neuromuscular transmission, and mitigated the disease by appropriate therapy.

Author Affiliations: Department of Neurology, Mayo Clinic, Rochester, Minnesota (Selcen, Shen, McEvoy, Engel); Division of Neurogenetics, Center for Neurological Diseases and Cancer, Nagoya University Graduate School of Medicine, Nagoya, Japan (Ohkawara, Ohno).

Corresponding Author: Andrew G. Engel, MD, Department of Neurology, Mayo Clinic, 200 First St SW, Rochester, MN 55905 (age@mayo.edu).

JAMA Neurol. 2015;72(8):889-896. doi:10.1001/jamaneurol.2015.0853
Published online June 8, 2015.

The development and maintenance of the neuromuscular junction depends crucially on the agrin-MuSK-LRP4 signaling system. Low-density lipoprotein receptor-related protein 4 (LRP4) and muscle-specific tyrosine kinase (MuSK) are anchored in the postsynaptic membrane. Agrin, secreted into the synaptic space by the nerve terminal, binds to multiple sites on the extracellular domain of LRP4, which then binds to the extracellular domain of MuSK on the postsynaptic membrane. This results in phosphorylation and activation of MuSK and clustering of MuSK and LRP4.[1,2] Activated MuSK, in concert with DOK7 and other postsynaptic proteins, acts on rapsyn to concentrate the acetylcholine receptor (AChR) in the postsynaptic membrane and promotes postsynaptic gene expression and differentiation. Clustered LRP4 also enhances presynaptic differentiation.[3]

Several reports have described congenital myasthenic syndromes (CMSs) caused by mutations in agrin[4-6] and MuSK,[7-11] but only 1 report has described mutations in LRP4.[12] This was the case of a 14-year-old girl with moderately severe fatigable limb-girdle weakness, dysplastic synaptic contacts, borderline end-plate (EP) AChR deficiency, smaller-than-normal individual EP regions, but no demonstrable defect of neuromuscular transmission at intercostal muscle EPs. The patient's weakness continued to progress, and by 24 years of age, she was barely able to walk. Herein we describe 2 young adult sisters with LRP4-related myasthenia caused by a novel homozygous LRP4 mutation. Intercostal muscle studies of the older sister reveal structurally and functionally abnormal EPs and EP AChR deficiency. Expression studies indicate that the mutant protein hinders LRP4 from binding to, activating, and phosphorylating MuSK.

Methods

Participants

All human studies were approved by the institutional review board of the Mayo Clinic in Rochester, Minnesota, and the 2 sisters (ie, patients) and 15 historical control participants provided written informed consent to participate in the studies. Intercostal muscle was obtained from the 15 historical control participants during chest surgery for unrelated diseases.

Genetic Analysis

Sanger sequencing for mutations in genes known to cause limb-girdle CMS (namely, *RAPSN*, *DOK7*, *GFPT1*, and *DPAGT1*) gave negative results. Next, exome sequencing of genomic DNA from both siblings was performed at the Mayo Clinic. The identified putative variants were scrutinized with Ingenuity Variant Analysis software (Qiagen). Variants at intergenic and intronic sites, and genes not expressed in skeletal muscle or the spinal cord based on the Gene Expression Omnibus database (http://www.ncbi.nlm.nih.gov/geo/), were excluded. The identified mutation was confirmed by Sanger sequencing of the family. Nucleotides of *LRP4* complementary DNA (cDNA) were numbered according to GeneBank accession number NM_002334.3.

To determine whether an identified nucleotide variant caused abnormal splicing, we isolated cDNA from the muscle specimens obtained from control participants and the 2 patients. To detect any alternative transcript, we amplified the cDNA from exons 25 to 29 and exons 26 to 28 with primers designed for the cDNA of the 2 patients and 2 control participants.

Structural Studies

Intercostal and serratus anterior muscle specimens were obtained from the older sister and from control participants without muscle disease undergoing thoracic surgery. Cryosections were used to colocalize the AChR and acetylcholinesterase as previously described.[13] End plates were localized for electron microscopy[14] and quantitatively analyzed[15] by established methods. Peroxidase-labeled α-bungarotoxin was used for the ultrastructural localization of AChR.[16] The number of AChRs per EP was measured with iodine 125-labeled α-bungarotoxin.[17]

In Vitro Electrophysiology Studies

Quantitative analysis of single EP regions was done for all 15 control participants and microelectrode studies of neuromuscular transmission and α-bgt binding sites per EP was conducted for 13 control participants. Intracellular microelectrode studies were performed on an intercostal muscle specimen obtained from the 34-year-old sister (patient 1). The amplitude of the miniature EP potential (MEPP) and the quantal content of the EPP (*m*) were determined as previously described.[18-20]

Plasmids

We used the following previously constructed plasmids: (1) full-length human *LRP4* cDNA for the luciferase assay and cell surface binding assays; (2) mouse *Musk* cDNA for luciferase assay; (3) the extracellular domain of mouse *Musk* cDNA and a fraction (amino acids 1141-1937) of rat *Agrn* cDNA, both of which were fused to an myc-tag and alkaline phosphatase (MuSKect-mycAP and agrin-mycAP) for cell surface binding assay; and (4) human *MUSK* cDNA with a flag-tag at the N-terminal end for coimmunoprecipitation assay. Mutant *LRP4* plasmid carrying p.Glu1233Ala was generated by the QuikChange Site-Directed Mutagenesis kit (Stratagene).[12] The ATF2-luciferase (ATF2-luc) reporter[12] and the phRL-TK Renilla luciferase vector (Promega) were used for the luciferase reporter assay.

Cell Cultures

HEK293 and COS7 cells were cultured in the Dulbecco Modified Eagle Medium supplemented with 10% fetal calf serum, and transfected with FuGENE 6 transfection reagent (Roche). The agrin-mycAP and MuSKect-mycAP proteins were produced as previously described.[12] Recombinant rat C-terminal agrin (10 ng/mL; R&D Systems) was used for agrin treatment, except for the cell-binding assays.

Luciferase Assays

We used an ATF2-luc reporter to monitor MuSK activation. The basis for this approach is that agrin induces JNK activation in myotubes[21] and that a previous report[22] has demonstrated in-

teraction between JNK and ATF2. This suggested that reporters regulated by JNK might reflect MuSK activation. We therefore tested several JNK reporters and found that ATF2-luc reporter responded to MuSK, LRP4, and agrin in a dose-dependent manner.[12]

HEK293 cells were transfected with ATF2-luc and phRL-TK along with the *MUSK* cDNA and the *LRP4* cDNA. Cells were cultured for 24 hours in a 96-well plate with or without 10 ng/mL of agrin in the medium. Cells were lysed with the Passive Lysis Buffer (Promega) and assayed for luciferase activity using the Dual-Luciferase Reporter Assay System (Promega). Each experiment was performed in triplicate.

Western Blotting

HEK293 cells transfected with MuSK and LRP4 plasmids were cultured for 24 hours in the presence of 10 ng/mL of agrin, as previously described.[12] The primary antibodies were mouse monoclonal anti-FLAG M2 (Sigma-Aldrich; F3165, dilution 1:4000), anti-β-actin (Santa Cruz Biotechnology; sc-47778, dilution 1:200), and the goat polyclonal anti-LRP4 (Abcam; ab85697, dilution 1:1000). The secondary antibodies were goat antimouse IgG (GE Healthcare; NA931V, dilution 1:6000) and mouse antigoat IgG (Santa Cruz Biotechnology; sc-2345, dilution 1:6000) conjugated to horseradish peroxidase.

Biotinylation Assay

HEK293 cells transfected with plasmids harboring wild-type LRP4 or its Glu1233Ala mutant were cultured for 48 hours. Cell surface proteins were isolated by biotinylating the cell surface proteins and precipitating the bound proteins with streptavidin beads, as previously described.[12]

Results

Clinical Data

Two young adult sisters with CMS (patient 1 in her mid-30s and patient 2 in her early 20s) who were born to nonconsanguineous parents, were investigated. Their parents and other siblings are unaffected.

Patient 1 was born after normal gestation and delivery. months. Developmental milestones (sitting and walking) were slightly delayed; after beginning to walk, she fell frequently. As a young child, she had mild difficulty chewing and swallowing. She never climbed steps or kept up with her peers in physical activities. Her weakness worsened around her menses. In her teens, she could only walk a short distance with support and became dependent on a wheelchair. On initial examination, she could barely rise from the sitting position without support, and her gait was waddling, hyperlordotic, and intoeing. Her weakness was confined to the axial and limb muscles with selective severe involvement of the dorsal forearm muscles. Her tendon reflexes were hypoactive. Her vital capacity was reduced to 49%, and the maximal inspiratory and expiratory pressures were reduced to 43% and 22% of normal, respectively. Repetitive nerve stimulation at 2 Hz revealed a decremental response of 37% in the trapezius and of 14% in facial muscles of the fourth compared with the first evoked compound muscle action potential (CMAP) (normal, <10%). Repetitive CMAPs, typical of the slow-channel myasthenic syndrome or EP acetylcholinesterase deficiency,[23] were absent. Brief strenuous exercise did not appreciably improve the decremental response or potentiate the first evoked CMAP as in the CMS-caused synaptotagmin-2 deficiency,[24] in some patients harboring mutations in agrin,[6] or in the Lambert-Eaton syndrome.[23] Needle electromyographic studies of multiple muscles revealed an increased proportion of short-duration, polyphasic motor unit potentials without spontaneous electrical activity, a common finding in myasthenic disorders owing to a variable proportion of muscle fibers in motor units failing to generate an action potential.

After treatment with 4 mg of albuterol sulfate twice daily for 1 week, patient 1 rose up from the sitting position 10 times without support, and the electromyographic decrement in her trapezius muscle decreased to 25%. One week later, she climbed 10 steps, walked 450 m (500 yd), and was able to groom herself independently. Additional treatment with pyridostigmine bromide or 3,4-diaminopyridine made her weaker and had to be discontinued.

Patient 2 appeared normal at birth and during infancy. She walked at a developmentally appropriate age but never learned to run or jump, found it difficult to climb steps, and could not keep up with her peers in physical activities. By late adolescence, her arm-elevation time was 22 seconds, and her gait was lordotic and waddling; she required assistance to rise from a sitting position and could climb only 20 steps before having to rest. There was mild weakness of the cervical and proximal arm muscles and mild to moderately severe weakness of the hip girdle muscles. Her tendon reflexes were hypoactive. Respiratory function tests showed that her vital capacity was reduced to 68% and that her maximal inspiratory and expiratory pressures were reduced to 39% and 47% of normal, respectively. After treatment with 4 mg of albuterol twice daily for 2 weeks, her arm and cervical muscles were of normal strength, her arm-elevation time was 60 seconds, and she could climb 44 steps before having to rest. Additional treatment with 60 mg of pyridostigmine twice daily over the next 2 years neither improved nor worsened her condition. A needle electromyographic examination suggested a mild proximal myopathy. After receiving albuterol for 2 years, repetitive stimulation of multiple muscles revealed no significant decrement of the evoked CMAP.

Structural Studies

Structural studies were performed in patient 1. Light microcopy revealed markedly diminished EP size. In transverse frozen sections reacted for acetylcholinesterase, the median length of 34 EPs was 7.2 μm (**Figure 1**A, B, E, and F); the median length of 69 EPs of 3 control participants was 21.3 μm ($P < .001$, determined by the use of the rank sum test) (Figure 1C, D, G, and H). Paired fluorescence localization studies revealed reduced synaptic expression of acetylcholinesterase and of the AChR in the EPs of patient 1 (Figure 1E and F) compared with the EPs in the 3 control participants (Figure 1G and H).

Qualitative inspection of 15 EP regions revealed 7 postsynaptic regions unoccupied or partially occupied by the nerve

Figure 1. Structural Observations

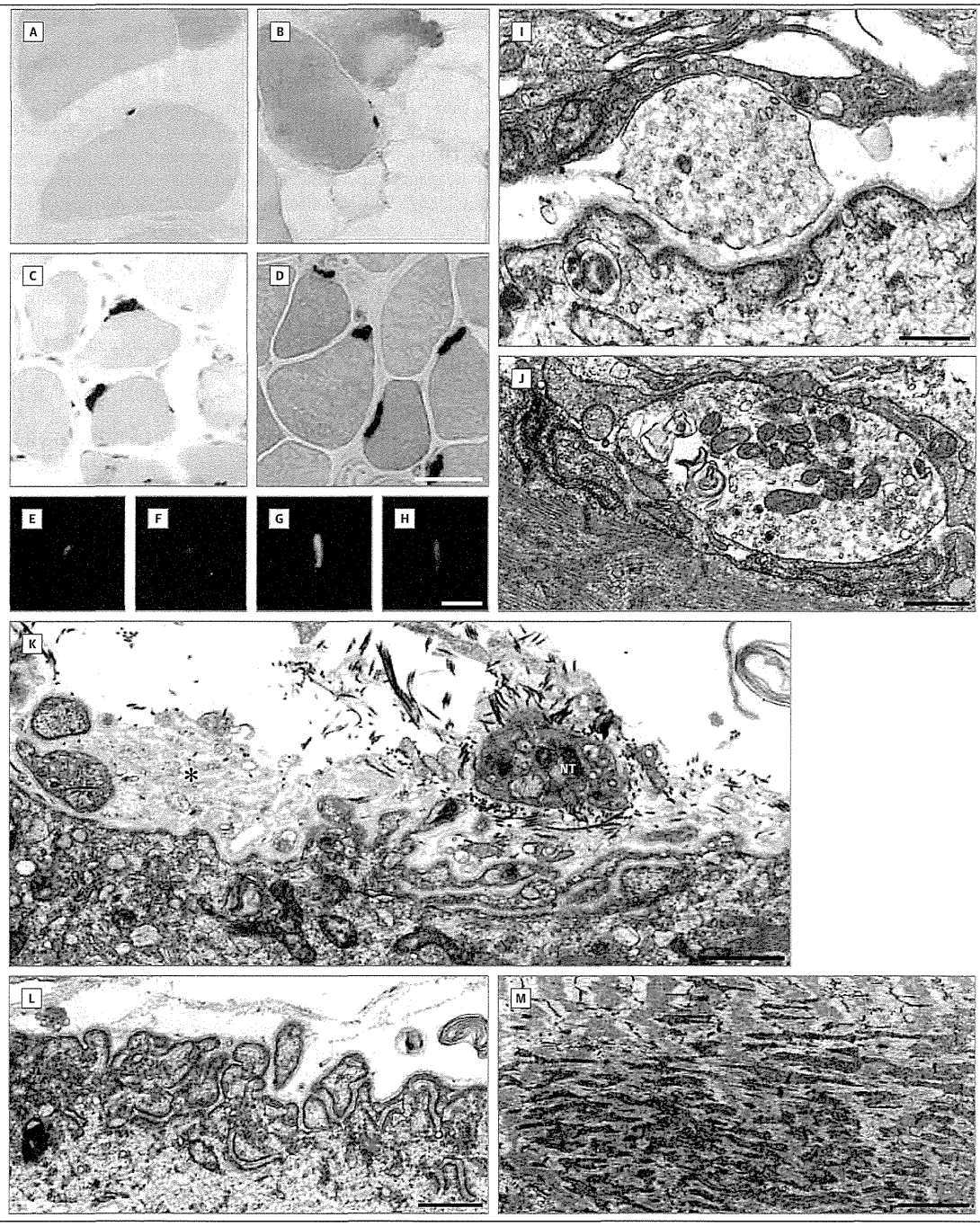

In transverse sections, the length of acetylcholinesterase (AChE)-reacted end-plate (EP) regions is markedly reduced in the EPs of patient 1 (A and B) compared with the EPs of control participants (C and D). Paired fluorescence studies reveal reduced expression of AChE (green) and acetylcholine receptors (AChRs) (red) in the EPs of patient 1 (E and F) compared with the EPs of control participants (G and H). Electron microscopy reveals simplified postsynaptic regions (I and J) and patchy expression of AChRs (black reaction product) at the EP (J). K, Electron microscopy also reveals a degenerating nerve terminal (NT) separated from a shallow postsynaptic region by a synaptic space containing coarse collagen fibrils; the region on the left shows a degenerate postsynaptic region displaying basal lamina remnants of preexisting folds (asterisk) and no NT. Electron microscopy also reveals a noninnervated postsynaptic region (L) and focal myofibrillar degeneration (M). Scale bars: A-D, 50 μm; E-H, 20 μm; I-L, 1 μm; M, 2 μm.

Table 1. Quantitative Analysis of Single EP Regions[a]

Measure	Control Participants (n = 15) Mean (SE)	EP Regions, No.	Older Sister Mean (SE)	EP Regions, No.	P Value
Nerve terminal area, μm^2	3.88 (0.39)	63	3.19 (0.76)	11	.59
Postsynaptic membrane length, μm	54.9 (5.3)	47	18.2 (2.00)	15	<.001
Postsynaptic area, μm^2	10.6 (0.79)	59	7.07 (1.02)	15	<.05
Postsynaptic membrane density, μm/μm^2	5.83 (0.25)	47	2.88 (0.23)	15	<.001

[a] More than 1 region can occur at a single end plate (EP).

Table 2. Microelectrode Studies of Neuromuscular Transmission and α-bgt Binding Sites per EP

Measure	Control Participants (n = 13) Mean (SE)	Participants or EPs,[a] No.	Older Sister Mean (SE)	EPs, No.	P Value[b]
EPP amplitude, mV	28.76 (1.98)	10[c]	4.66 (0.74)	13	<.001
MEPP amplitude, mV	1.00 (0.03)	165[d]	0.43 (0.078)	13[e]	<.001
Quantal content of EPP at 1 Hz (*m*)[f]	26.9 (1.0)	91	10.8 (2.36)	13	<.001
[^{125}I]α-bgt binding sites per EP, No.	12.8 × 10^6 (0.8 × 10^6)	13	3.03 × 10^6	1	<.001[g]

Abbreviations: EP, end plate; [^{125}I]α-bgt, iodine 125–labeled α-bungarotoxin; MEPP, miniature EP potential.

[a] Number of participants for EPP amplitudes and [^{125}I]α-bgt binding sites, and number of EPs for MEPP and *m*.

[b] Determined by use of 2-tailed *t* test.

[c] Control EPP amplitudes estimated from the product of *m* and the MEPP amplitude.

[d] Corrected for a membrane potential of −80 mV and a fiber diameter of 50 μm (30°C).

[e] Estimated from quantal component of EPP.

[f] Corrected for a membrane potential of −80 mV, nonlinear summation, and non-Poisson release.

[g] Determined by use of 1-sample 1-tailed *t* test.

terminal (Figure 1K and L) and 2 regions displaying degenerating junctional folds (Figure 1K). In contrast, at 157 EP regions of control participants, only 15 postsynaptic regions were unoccupied by the nerve terminal ($P < .001$, determined by use of the rank sum test), and only 6 postsynaptic regions displayed degenerating folds ($P < .03$, determined by use of the *z* score). Most postsynaptic regions had poorly developed junctional folds (Figure 1I and J), and a single nerve terminal was degenerating (Figure 1K). The postsynaptic reaction for AChR, revealed by peroxidase-labeled α-bungarotoxin, was attenuated (Figure 1J). At the light microscopic level, the intercostal muscle specimen showed a single-target formation and small focal decreases of enzyme activity. Consistent with this, at the electron microscopic level, occasional muscle fibers displayed focal myofibrillar degeneration (Figure 1M) that is likely secondary to functional denervation. Morphometric analysis revealed that the size of the nerve terminal was not significantly different from normal but that the postsynaptic area was reduced by 33% (ie, 67% of normal) and that the postsynaptic membrane density was reduced by 50% (ie, 50% of normal) (Table 1).

In Vitro Analysis of Neuromuscular Transmission

The evoked EPPs were subthreshold to trigger action potentials and were recorded without curare. The mean values for the EPP amplitude, the quantal content of the EPP (*m*), and the amplitude of the MEPP derived from the quantal component of the EPP were reduced to 16%, 40%, and 43%, respectively, of the corresponding mean values for the control participants. The mean number of AChRs per EP, determined from the number of α-bungarotoxin binding sites, was decreased to 25% of the mean number for the control participants (Table 2).

Mutation Analysis

Whole-exome sequencing in both patients (confirmed by Sanger sequencing) revealed a novel homozygous p.Glu1233Ala (c.3698A>C) mutation in exon 26 (Figure 2). The mutated residue is positioned at the edge of the third β-propeller domain of LRP4 and close to the conserved YWTD motif important for β-sheet formation. The unaffected brother and the mother are heterozygous for the mutation. Glu1233 is highly conserved across vertebrates, but not in insects, and is not reported in the Exome Variant Database (Exome Variant Server, National Heart, Lung, and Blood Institute Grand Opportunity Exome Sequencing Project, Seattle, Washington [http://evs.gs.washington.edu/EVS/]; January 2015), and it is predicted to be disease causing by MutationTaster but benign by Polymorphism Phenotyping v2. Interestingly, mutations in the central cavity of the third β-propeller domain of *LRP4* were previously reported to impair Wnt signaling and cause bone disease, including Cenani-Lenz syndactyly syndrome[25] and sclerosteosis-2.[26]

Because the A>C variant is the penultimate nucleotide of exon 26 and because MutationTaster predicts it to alter splicing, we isolated cDNA from the patient's intercostal and serratus anterior muscles and amplified the segment, including exon 26 by 2 different sets of primers. In both specimens, the mutant residue was homozygous, and there was no evidence for abnormal splicing.

Figure 2. Structure of and Identified Mutations in *LRP4*

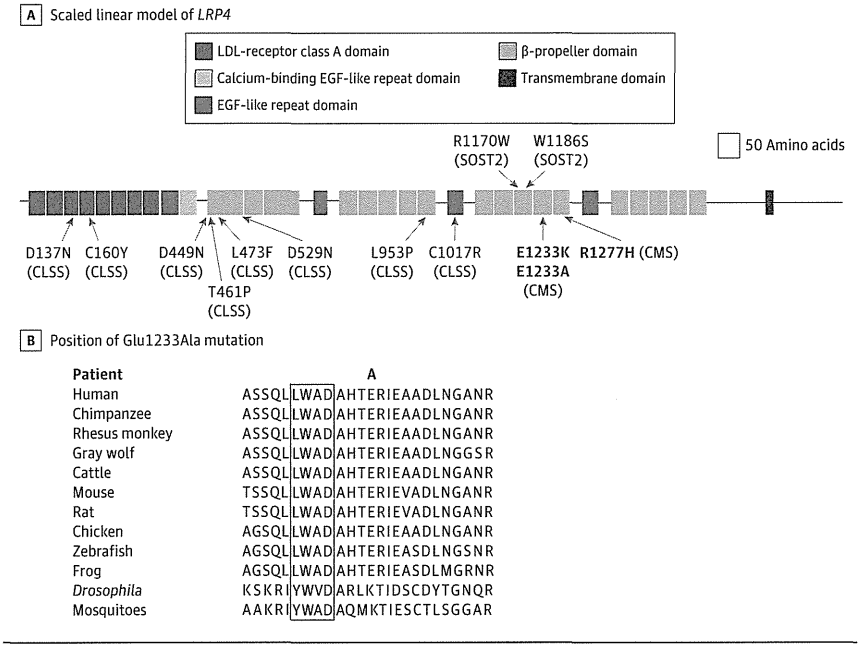

A, Scaled linear model of *LRP4* with color-coded domains and identified mutations. Mutations causing congenital myasthenic syndrome (CMS) are shown in red letters; mutations causing Cenani-Lenz syndactyly syndrome (CLSS) and sclerosteosis-2 (SOST2) are shown in black letters. B, The Glu1233Ala mutation is in a highly conserved domain of *LRP4* and the blue box encloses a motif conserved in all species. The substituting Ala, indicated by the red A, is 4 residues downstream of this motif. Glu1233 is highly conserved across vertebrates but not in insects. EGF indicates *epidermal growth factor*.

Expression Studies

Expression studies show that Glu1233Ala inhibits the MuSK signaling pathway. During the formation of the neuromuscular junction, binding of agrin to LRP4 induces phosphorylation and activation of MuSK.[3] Activated MuSK activates ATF2 downstream of JNK to induce clustering of AChRs.[12,27] To investigate the effect of the Glu1233Ala mutation on this signaling pathway, we used a JNK-responsive ATF2-luc reporter that specifically monitors MuSK-dependent stimulation in transfected HEK293 cells.[27] When LRP4 and MuSK are overexpressed, limited ATF2 activation occurs even in the absence of agrin.[12] The addition of agrin to this system further enhances ATF2 activation by wild-type LRP4, whereas activation of ATF2 by mutant LRP4 is markedly attenuated (**Figure 3**A). We found that both the previously reported Glu1233Lys mutation[12] (Figure 3B) and the currently identified Glu1233Ala mutation (Figure 3A) compromise ATF2 activation, but the activation is consistently lower with Glu1233Ala than with Glu1233Lys.

In another experiment using HEK293 cells, we examined the effects of wild-type and mutant LRP4 on MuSK phosphorylation that occurs during the assembly of the agrin-LRP4-MuSK complex. Consistent with its effects on MuSK signaling activity, mutant LRP4 compromises agrin-enhanced MuSK phosphorylation (Figure 3C). Both experiments support the notion that Glu1233Ala in LRP4 compromises agrin-mediated activation of MuSK.

MuSK and agrin bind to different extracellular residues of LRP4.[3] We therefore examined the binding of MuSK and agrin to mutant and wild-type LRP4 expressed on the surface of COS cells. We first confirmed that both wild-type and mutant LRP4 are similarly expressed on the plasma membrane by use of the biotinylation assay (Figure 3D). We then overlaid recombinant human MuSKect-AP and recombinant human neural agrin-AP on COS cells expressing LRP4. Measurement of alkaline phosphatase activity revealed that MuSK and agrin bind efficiently to wild-type LRP4 but not to mutant LRP4 (Figure 3E). Thus, all 3 experiments indicate that Glu1233Ala in LRP4 inhibits agrin-mediated upregulation of MuSK signaling.

Discussion

The 2 sisters described in this report harbor a homozygous p.Glu1233Ala mutation in the third propeller domain of LRP4 that binds to and activates MuSK. An intercostal muscle biopsy of the older sister revealed very small EPs with poorly developed postsynaptic regions, and postsynaptic regions that were degenerating or denuded of their nerve terminal. The amplitude of the EPP was reduced to 16% of normal owing to the combined decrease of the quantal content of the EPP and of the MEPP amplitude (Table 2). The decreased amplitude of the MEPP can be attributed to decreased input resistance of the EP owing to simplification of the postsynaptic membrane, as well as the attenuated expression of AChRs on the remaining junctional folds. The decreased quantal content of the EPP is adequately explained by the small size of individual EPs, and hence of the total number of synaptic vesicles available for release by nerve impulse. Thus, the observed structural and electrophysiologic abnormalities are consistent with an abrogated role played by LRP4 in the development and maintenance of the neuromuscular junction.[3]

Figure 3. Expression Studies

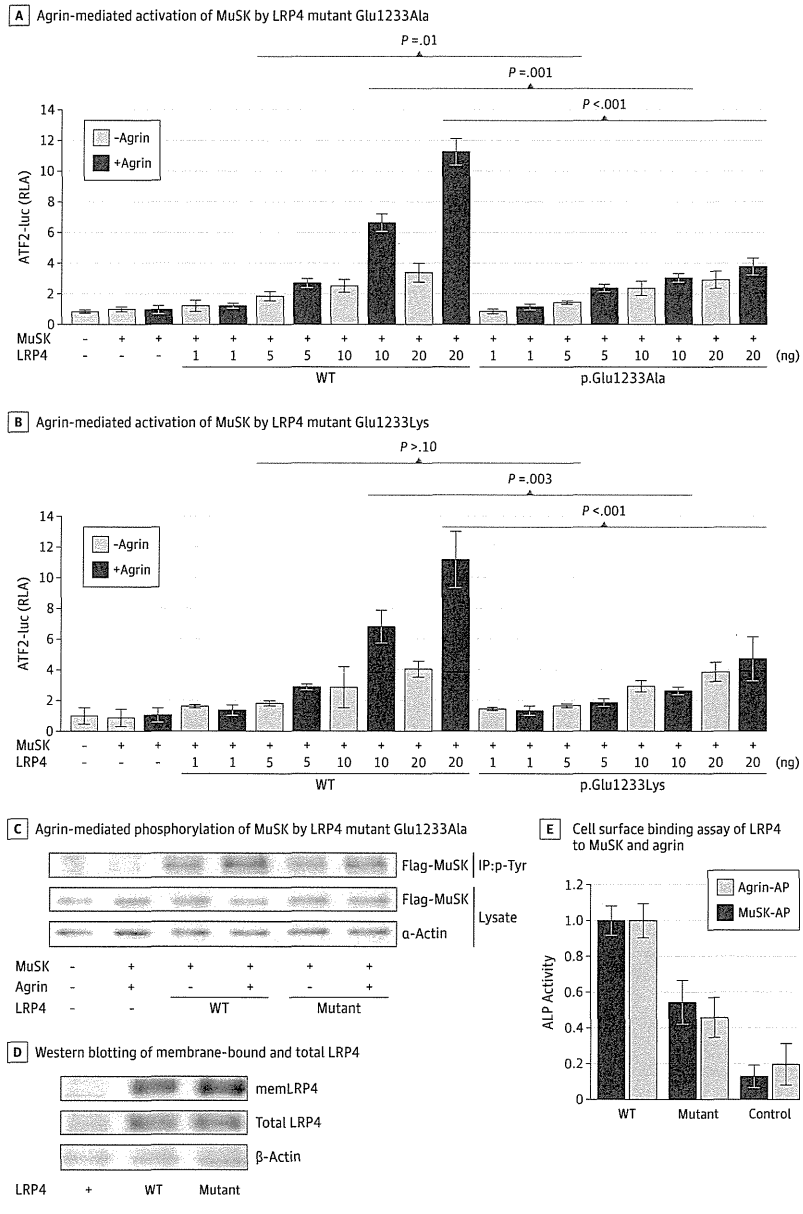

The lipoprotein receptor-related protein 4 (LRP4) mutants Glu1233Ala (A) and Glu1233Lys (B) inhibit agrin-mediated upregulation of muscle-specific tyrosine kinase (MuSK) signaling. Agrin-mediated upregulation of MuSK signaling in HEK293 cells is monitored by the ATF2-luciferase (ATF2-luc) reporter assay. Cells were transfected with the ATF2-luc and Renilla reporter plasmids, along with MuSK complementary DNA (cDNA) and wild-type (WT) or mutant LRP4, and then incubated with or without 10 ng/mL of agrin. Error bars indicate mean (SD) values (n=3) of relative luciferase activity (RLA) calculated by dividing the firefly luciferase activity by the Renilla luciferase activity, which is further normalized for activity without MuSK and LRP4. C, Effect of mutant and WT LRP4 on MuSK phosphorylation in HEK293 cells transfected with Flag-MuSK and the indicated LRP4 cDNA with or without agrin (10 ng/mL). Phosphorylated MuSK was detected by immunoprecipitation of cell lysate by antiphosphotyrosine antibody (IP:p-Tyr) followed by immunoblotting with anti-FLAG antibody. Wild-type LRP4 phosphorylates MuSK, which is further enhanced by agrin. Mutant LRP4 abolished responsiveness to agrin. D, Western blotting detected membrane-bound LRP4 (memLRP4) and total LRP4. Membrane proteins were biotinylated and precipitated with streptavidin. β-Actin in each sample serves as a loading control. E, The LRP4 mutant impairs binding of LRP4 to MuSK and agrin in cell surface binding assays. COS7 cells were transfected with the WT or mutant LRP4 cDNA and treated with a concentrated conditioned medium containing either neural agrin-mycAP or MuSKect-mycAP, both of which expressed an alkaline phosphatase (ALP) fusion protein. Control cells were transfected with an empty vector. The error bars indicate mean (SD) of ALP activity of bound agrin-mycAP and MuSKect-mycAP in 3 independent wells. Mutant LRP4 reduces binding of MuSKect-mycAP and agrin-mycAP.

Conclusions

The first reported patient with LRP4-related myasthenia harbored 2 heterozygous mutations in LRP4, p.Glu1233Lys and p.Arg1277His. At 14 years of age, her synaptic contacts were dysplastic, the individual EP regions were smaller than normal, and the EP AChR content slightly reduced, but, paradoxically, in vitro electrophysiology studies of intercostal muscle EPs revealed no abnormality.[12] Interestingly, expression studies of both mutant proteins in the first patient[12] and of the single mutant protein in the 2 sisters in this study revealed impaired LRP4 binding to, activating, and phosphorylating MuSK. The reason for the much milder clinical, structural, and electrophysiologic abnormalities observed in the first identified patient with LRP4-related myasthenia compared with the patients described in this report remains unknown. We initially attributed the milder findings in the first reported patient to

relative sparing of the intercostal muscles. Alternatively, the structural and physiologic abnormalities at the EPs in LRP4-related myasthenia could worsen with age, consistent with the progressive clinical course in all 3 LRP4-deficient patients observed to date. The greater suppression of ATF2 activation by the Glu1233Ala mutation in LRP4 than by the previously reported Glu1233Lys mutation in LRP4 likely also contributes to the phenotypic differences between the first reported patient and the 2 patients described herein. Finally, single-nucleotide polymorphisms in modifier genes may also contribute to phenotypic differences. That both kinships harbor mutations at the edge of the third β-propeller domain and that 2 of the 3 identified mutations occur at codon 1233 suggest a hot spot for causing CMS.

ARTICLE INFORMATION

Accepted for Publication: April 6, 2015.

Published Online: June 8, 2015. doi:10.1001/jamaneurol.2015.0853.

Author Contributions: Dr Engel had full access to all of the data in the study and takes responsibility for the integrity of the data and the accuracy of the data analysis.
Study concept and design: Selcen, Shen, Ohno, Engel.
Acquisition, analysis, or interpretation of data: All authors.
Drafting of the manuscript: Selcen, Ohno, Engel.
Critical revision of the manuscript for important intellectual content: All authors.
Statistical analysis: Shen, Engel.
Obtained funding: Selcen, Ohkawara, Ohno, Engel.
Administrative, technical, or material support: Ohno, Engel.
Study supervision: Ohno, Engel.

Conflict of Interest Disclosures: None reported.

Funding/Support: This work was supported by National Institutes of Health grant NS62777 (Dr Engel), the Mayo Clinic Center for Individualized Medicine, and by Grants-in-Aid from the Ministry of Education, Culture, Sports, Science and Technology and Ministry of Health, Labour and Welfare of Japan (Drs Ohkawara and Ohno).

Role of Funder/Sponsor: The funding sources had no role in the design and conduct of the study; collection, management, analysis, or interpretation of the data; preparation, review, or approval of the manuscript; and decision to submit the manuscript for publication.

REFERENCES

1. Kim N, Stiegler AL, Cameron TO, et al. Lrp4 is a receptor for Agrin and forms a complex with MuSK. *Cell*. 2008;135(2):334-342.

2. Zhang B, Luo S, Wang Q, Suzuki T, Xiong WC, Mei L. LRP4 serves as a coreceptor of agrin. *Neuron*. 2008;60(2):285-297.

3. Burden SJ, Yumoto N, Zhang W. The role of MuSK in synapse formation and neuromuscular disease. *Cold Spring Harb Perspect Biol*. 2013;5(5):a009167.

4. Huzé C, Bauché S, Richard P, et al. Identification of an agrin mutation that causes congenital myasthenia and affects synapse function. *Am J Hum Genet*. 2009;85(2):155-167.

5. Maselli RA, Fernandez JM, Arredondo J, et al. LG2 agrin mutation causing severe congenital myasthenic syndrome mimics functional characteristics of non-neural (z-) agrin. *Hum Genet*. 2012;131(7):1123-1135.

6. Nicole S, Chaouch A, Torbergsen T, et al. Agrin mutations lead to a congenital myasthenic syndrome with distal muscle weakness and atrophy. *Brain*. 2014;137(pt 9):2429-2443.

7. Chevessier F, Faraut B, Ravel-Chapuis A, et al. MUSK, a new target for mutations causing congenital myasthenic syndrome. *Hum Mol Genet*. 2004;13(24):3229-3240.

8. Mihaylova V, Salih MA, Mukhtar MM, et al. Refinement of the clinical phenotype in musk-related congenital myasthenic syndromes. *Neurology*. 2009;73(22):1926-1928.

9. Maselli RA, Arredondo J, Cagney O, et al. Mutations in MUSK causing congenital myasthenic syndrome impair MuSK-Dok-7 interaction. *Hum Mol Genet*. 2010;19(12):2370-2379.

10. Ben Ammar A, Soltanzadeh P, Bauché S, et al. A mutation causes MuSK reduced sensitivity to agrin and congenital myasthenia. *PLoS One*. 2013;8(1):e53826.

11. Maggi L, Brugnoni R, Confalioneri P, et al. Marked phenotypic variability in two siblings affected by congenital myasthenic syndrome caused by mutations in MUSK. *J Neurol*. 2013;260(11):2894-2896.

12. Ohkawara B, Cabrera-Serrano M, Nakata T, et al. LRP4 third β-propeller domain mutations cause novel congenital myasthenia by compromising agrin-mediated MuSK signaling in a position-specific manner. *Hum Mol Genet*. 2014;23(7):1856-1868.

13. Fambrough DM, Engel AG, Rosenberry TL. Acetylcholinesterase of human erythrocytes and neuromuscular junctions: homologies revealed by monoclonal antibodies. *Proc Natl Acad Sci U S A*. 1982;79(4):1078-1082.

14. Engel AG. The muscle biopsy. In: Engel AG, Franzini-Armstrong C, eds. *Myology*. 3rd ed. New York, NY: McGraw-Hill; 2004:681-690.

15. Engel AG. Quantitative morphological studies of muscle. In: Engel AG, Franzini-Armstrong C, eds. *Myology*. 2nd ed. New York, NY: McGraw-Hill; 1994:1018-1045.

16. Engel AG, Lindstrom JM, Lambert EH, Lennon VA. Ultrastructural localization of the acetylcholine receptor in myasthenia gravis and in its experimental autoimmune model. *Neurology*. 1977;27(4):307-315.

17. Engel AG. The investigation of congenital myasthenic syndromes. *Ann N Y Acad Sci*. 1993;681:425-434.

18. Elmqvist D, Quastel DMJ. A quantitative study of end-plate potentials in isolated human muscle. *J Physiol*. 1965;178(3):505-529.

19. Engel AG, Nagel A, Walls TJ, Harper CM, Waisburg HA. Congenital myasthenic syndromes: I, deficiency and short open-time of the acetylcholine receptor. *Muscle Nerve*. 1993;16(12):1284-1292.

20. Uchitel O, Engel AG, Walls TJ, Nagel A, Atassi MZ, Bril V. Congenital myasthenic syndromes: II, syndrome attributed to abnormal interaction of acetylcholine with its receptor. *Muscle Nerve*. 1993;16(12):1293-1301.

21. Weston C, Yee B, Hod E, Prives J. Agrin-induced acetylcholine receptor clustering is mediated by the small guanosine triphosphatases Rac and Cdc42. *J Cell Biol*. 2000;150(1):205-212.

22. Gupta S, Campbell D, Dérijard B, Davis RJ. Transcription factor ATF2 regulation by the JNK signal transduction pathway. *Science*. 1995;267(5196):389-393.

23. Harper CM. Electrodiagnosis of myasthenic disorders. In: Engel AG, et al. *Myasthenia Gravis and Myasthenic Disorders*. 2nd ed. New York, NY: Oxford; 2012:37-59.

24. Herrmann DN, Horvath R, Sowden JE, et al. Synaptotagmin 2 mutations cause an autosomal-dominant form of Lambert-Eaton myasthenic syndrome and nonprogressive motor neuropathy [published correction appears in *Am J Hum Genet*. 2014;95(4):472]. *Am J Hum Genet*. 2014;95(3):332-339.

25. Li Y, Pawlik B, Elcioglu N, et al. LRP4 mutations alter Wnt/beta-catenin signaling and cause limb and kidney malformations in Cenani-Lenz syndrome. *Am J Hum Genet*. 2010;86(5):696-706.

26. Leupin O, Piters E, Halleux C, et al. Bone overgrowth-associated mutations in the *LRP4* gene impair sclerostin facilitator function. *J Biol Chem*. 2011;286(22):19489-19500.

27. Ohkawara B, Niehrs C. An ATF2-based luciferase reporter to monitor non-canonical Wnt signaling in *Xenopus* embryos. *Dev Dyn*. 2011;240(1):188-194.

SCIENTIFIC REPORTS

OPEN

SRSF1 and hnRNP H antagonistically regulate splicing of *COLQ* exon 16 in a congenital myasthenic syndrome

Received: 24 March 2015
Accepted: 22 July 2015
Published: 18 August 2015

Mohammad Alinoor Rahman[1], Yoshiteru Azuma[1], Farhana Nasrin[1], Jun-ichi Takeda[1], Mohammad Nazim[1], Khalid Bin Ahsan[1], Akio Masuda[1], Andrew G. Engel[2] & Kinji Ohno[1]

The catalytic subunits of acetylcholinesterase (AChE) are anchored in the basal lamina of the neuromuscular junction using a collagen-like tail subunit (ColQ) encoded by *COLQ*. Mutations in *COLQ* cause endplate AChE deficiency. An A-to-G mutation predicting p.E415G in *COLQ* exon 16 identified in a patient with endplate AChE deficiency causes exclusive skipping of exon 16. RNA affinity purification, mass spectrometry, and siRNA-mediated gene knocking down disclosed that the mutation disrupts binding of a splicing-enhancing RNA-binding protein, SRSF1, and *de novo* gains binding of a splicing-suppressing RNA-binding protein, hnRNP H. MS2-mediated artificial tethering of each factor demonstrated that SRSF1 and hnRNP H antagonistically modulate splicing by binding exclusively to the target in exon 16. Further analyses with artificial mutants revealed that SRSF1 is able to bind to degenerative binding motifs, whereas hnRNP H strictly requires an uninterrupted stretch of poly(G). The mutation compromised splicing of the downstream intron. Isolation of early spliceosome complex revealed that the mutation impairs binding of U1-70K (snRNP70) to the downstream 5′ splice site. Global splicing analysis with RNA-seq revealed that exons carrying the hnRNP H-binding GGGGG motif are predisposed to be skipped compared to those carrying the SRSF1-binding GGAGG motif in both human and mouse brains.

RNA splicing is a highly specialized process especially evolved in humans and other higher metazoans to achieve intricate regulation of gene expressions and to expand the proteome diversity. It is well established that misregulated splicing compromises the fidelity of biological processes and causes a plethora of human diseases. However, the precise molecular mechanisms of how a disease-causing mutation compromises the finely tuned splicing regulation have been dissected in only a limited number of genes. Elucidation of the mechanisms that cause abnormal splicing in human diseases also sheds light on the splicing code in the normal state, and can possibly lead to development of rational therapy.

Congenital myasthenic syndromes (CMSs) are a heterogeneous group of inherited neuromuscular disorders, which arise due to defects in genes encoding presynaptic, synaptic, and postsynaptic proteins expressed at the neuromuscular junction (NMJ)[1,2]. Acetylcholinesterase (AChE) encoded by *ACHE* rapidly terminates neuromuscular signal transmission by hydrolyzing the neurotransmitter acetylcholine (ACh). The predominant species of AChE at NMJ is the asymmetric A_{12} species[3] which comprises three tetramers of the $AChE_T$ isoform that are covalently attached to the triple helical collagen-like tail (ColQ). ColQ encoded by *COLQ* is essential for anchoring AChE to the NMJ. ColQ has three distinct domains: an N-terminal proline-rich domain organizing the catalytic AChE subunits into a tetramer, a collagen domain forming a triple helix and harboring two heparan-sulfate-proteoglycan-binding

[1]Division of Neurogenetics, Center for Neurological Diseases and Cancer, Nagoya University Graduate School of Medicine, Nagoya, Aichi, Japan. [2]Department of Neurology, Mayo Clinic, Rochester, MN, USA. Correspondence and requests for materials should be addressed to K.O. (email: ohnok@med.nagoya-u.ac.jp)

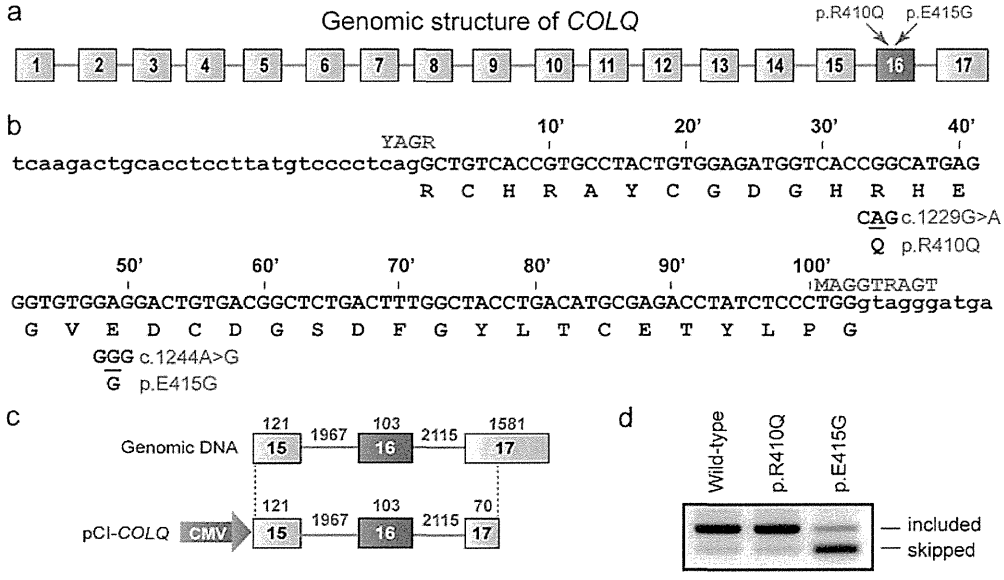

Figure 1. Genomic structure of *COLQ*, identified mutations, and their functional consequences. (**a**) Genomic structure (not drawn to scale) of human *COLQ* gene and two identified mutations in exon 16. (**b**) Nucleotide sequence of *COLQ* exon 16 (uppercase letters) and its flanking introns (lowercase letters). The two mutant nucleotides are underlined. Exonic positions are indicated above the sequence. The consensus sequences of U2-dependent 5′ splice site and 3′ splice site are shown in green letters (Y = C/T, R = A/G, M = A/C)[51]. (**c**) Structure of pCI-*COLQ* minigene. Genomic structure is not drawn to scale. The lengths of exons and introns are indicated in blue. (**d**) RT-PCR of *COLQ* minigene expressed in HeLa cells.

domains (HSPBD), and a C-terminal domain (CTD) enriched in charged amino acids and cysteines. Endplate AChE deficiency is caused by recessive mutations in the *COLQ* gene, but not by mutations in the *ACHE* gene encoding the catalytic subunit[4]. A number of mutations in *COLQ* are associated with endplate AChE deficiency[5]. Based on the position of the mutation and the effect on AChE expression, *COLQ* mutations can fall into four categories[6]: (1) N-terminal mutations compromising the association of $AChE_T$ with ColQ; (2) truncation mutations in the collagen domain disrupting the collagenic tail of AChE; (3) CTD missense mutations disrupting triple helical conformation of ColQ; and (4) CTD mutations affecting anchoring of ColQ at NMJ. We exploited specific binding of the HSPBD to perlecan[7] and of the CTD to MuSK[8] to develop a protein-anchoring therapy for *Colq*-knockout mice[9], but there is no rational therapy for human endplate AChE deficiency except for partial mitigation of the symptoms with ephedrine[10] or albuterol[11].

Serine/arginine-rich splicing factor 1 (SRSF1) is a ubiquitously expressed splicing factor of the serine (S)- and arginine (R)-rich protein family, which functions in both constitutive and alternative splicing[12]. SRSF1 also has a role in nonsense-mediated mRNA decay (NMD)[13], mRNA export[14], and translation[15]. *SRSF1* is also reported to be a proto-oncogene[16]. HnRNP H is a member of heterogeneous nuclear ribonucleoprotein (hnRNP) family, which has been reported to function exclusively in pre-mRNA splicing[17–20].

We previously reported a missense mutation (p.E415G) in the CTD of *COLQ* in a patient with endplate AChE deficiency, which causes aberrant skipping of a constitutively spliced exon 16 encoding a part of the ColQ CTD[21]. In this manuscript, we investigate the mechanism underlying aberrant exon skipping. We demonstrate that the mutation disrupts binding of a splicing-enhancing factor SRSF1, and gains a *de novo* binding affinity for a splicing-suppressing factor hnRNP H. We also find that the mutation impairs recruitment of U1 snRNP (U1-70K) to the downstream 5′ splice site.

Results

p.E415G in the CTD of ColQ causes skipping of exon 16. We previously reported two heteroallelic missense mutations in *COLQ* exon 16 in a patient with endplate AChE deficiency (Fig. 1a,b)[21]. We introduced p.R410Q (c.1229G > A) and p.E415G (c.1244A > G) into human *COLQ* cDNA and expressed mutant ColQ proteins in COS cells. We overlaid the purified mutant ColQ on the frog muscle sections, and found that p.R410Q caused loss of binding of ColQ to the frog endplate, whereas p.E415G had no effect on binding of ColQ to the frog endplate[21]. RT-PCR analysis revealed that p.E415G caused skipping of *COLQ* exon 16 in the patient muscle, indicating that p.E415G is not a missense mutation but a splicing mutation. Skipping of exon 16 (103 nt) causes a shift in the reading frame and deletes the C-terminal one-third of the CTD. We reported that similarly deleted or mutated CTDs are incompetent to bind to

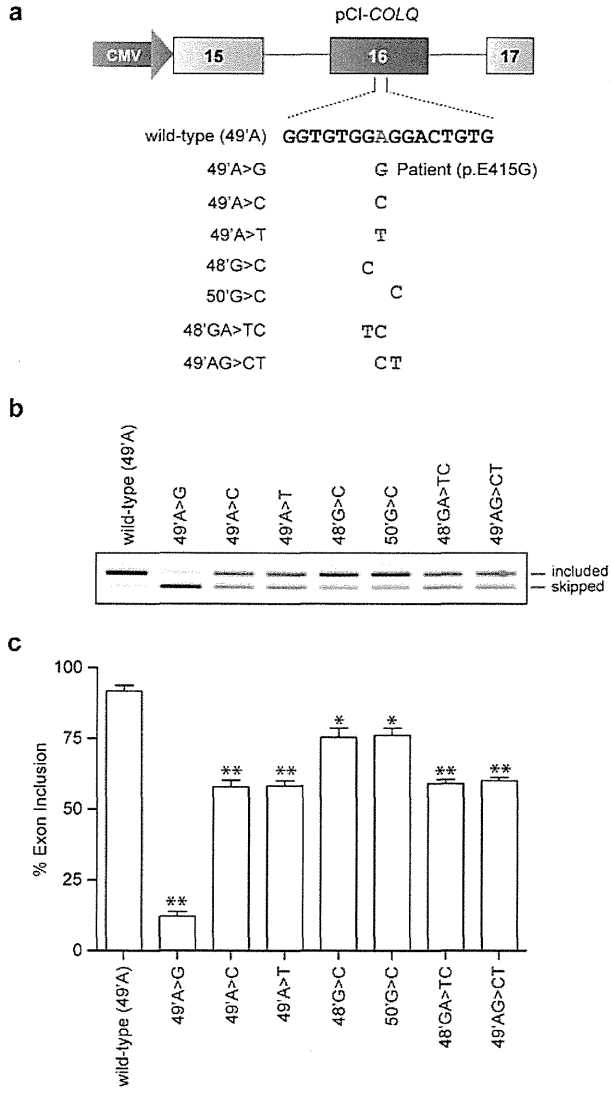

Figure 2. Construction of mutant minigenes and splicing assays. (**a**) Structure of pCI-*COLQ* minigene. The patient's mutation and six artificial mutations introduced into *COLQ* minigene are indicated. Exonic positions indicated in Fig. 1b are used. (**b**) RT-PCR of *COLQ* minigenes in HeLa cells. (**c**) Ratios of exon 16 inclusion are quantified with image J. Mean and standard deviation (SD) of three independent experiments are indicated. $^{**}p < 0.01$ and $^{*}p < 0.05$ compared to the wild-type minigene by Student's t-test.

MuSK and are incapable of being anchored to the NMJ[21,22]. In this study, we investigate the molecular basis of aberrant splicing due to p.E415G.

p.E415G disrupts an exonic splicing enhancer (ESE), and *de novo* generates an exonic splicing silencer (ESS). We first confirmed that a minigene spanning exons 15 and 17 expressed in HeLa cells recapitulates aberrant splicing (Fig. 1c,d). To examine whether the identified splicing mutation (p.E415G) disrupts an ESE or *de novo* generates an ESS, we engineered six artificial mutations at or around p.E415G (Fig. 2a). All mutants caused skipping of exon 16 with variable degrees (Fig. 2b,c), indicating that the A nucleotide at exonic position 49 and its neighboring nucleotides constitute an ESE. Among the analyzed mutations, the patient's mutation (G at exonic position 49) caused marked skipping of exon 16 compared to those observed with the other mutants, indicating that the patient's mutation possibly generates a *de novo* ESS.

p.E415G disrupts binding of SRSF1 and gains binding of hnRNP H. Having identified the essential nucleotides that constitute a splicing *cis*-element, we next searched for a splicing *trans*-factor responsible for splicing of exon 16. We employed RNA affinity purification of the HeLa nuclear extract with